IEEE Access
Multidisciplinary ⋮ Rapid Review ⋮ Open Access Journal

Received 25 February 2026, accepted 8 March 2026, date of publication 12 March 2026, date of current version 18 March 2026.

Digital Object Identifier 10.1109/ACCESS.2026.3673225

RESEARCH ARTICLE

Photovoltaic-Integrated Wireless Charging Systems for Electric Vehicles: A Smart City Perspective on Sustainable Urban Mobility

TAREQ ANWAR SHIKDAR[1] **AND HANNU LAAKSONEN**[2], **(Member, IEEE)**
[1]School of Technology and Innovations, University of Vaasa, FI-65200 Vaasa, Finland
[2]School of Technology and Innovations, Flexible Energy Resources, Electrical Engineering, University of Vaasa, FI-65200 Vaasa, Finland

Corresponding author: Hannu Laaksonen (hannu.laaksonen@uwasa.fi)

ABSTRACT The rapid growth of electric vehicles (EVs) necessitates charging infrastructures that are efficient, user-friendly, and compatible with renewable energy–driven smart-city ecosystems. Wireless power transfer (WPT) has emerged as a promising alternative to conventional plug-in charging by enabling contactless, automated, and safer energy delivery. In this work, a comprehensive photovoltaic (PV)-integrated wireless charging system (WCS) for EVs is proposed and evaluated through detailed MATLAB/Simulink simulations. The system integrates PV generation with maximum power point tracking (MPPT), battery energy storage supported by bidirectional DC–DC conversion, and a Series–Series (SS) compensated inductive coupling network operating near 85 kHz. Two three-phase configurations are investigated: a static fast-charging system rated at approximately 4 kW for residential single-vehicle applications and a stationary/dynamic charging system delivering approximately 31.5 kW in total for multi-vehicle and public transportation scenarios. Simulation results demonstrate stable operation across all power-conditioning stages, effective energy coordination between PV and battery subsystems, and high wireless transfer performance, with coil-to-coil efficiency reaching approximately 91.7% and overall system efficiencies of about 80% and 90% for the two configurations, respectively. The inclusion of a DC–DC buck converter and an integrated Battery Management System (BMS) ensures smooth voltage and current regulation, safe battery operation, and reliable charging behavior. From a system-level perspective, the proposed PV-integrated WCS can reduce dependence on grid power, alleviate stress on urban distribution networks, and support decentralized, renewable-powered EV charging. The presented framework demonstrates the technical feasibility and practical potential of wireless charging as a key enabler of sustainable and resilient smart-city mobility infrastructures.

INDEX TERMS Electric vehicles (EVs), wireless power transfer (WPT), photovoltaic (PV) integration, series–series (SS) compensation topology, dynamic wireless charging, smart cities.

I. INTRODUCTION

Greenhouse gases such as carbon dioxide (CO_2) [1], nitrous oxides, methane, and fluorinated gases [2] remain major contributors to global warming and climate instability. Fossil-fuel combustion accelerates greenhouse gas accumulation and environmental degradation [3], while internal combustion engine (ICE) vehicles continue to represent a major share of global emissions [4]. Increasing climate concerns, rising energy insecurity, and stricter emission regulations have therefore accelerated the global transition toward electric vehicles (EVs) as sustainable transportation solutions [5], [6]. However, large-scale EV adoption requires charging infrastructures that are efficient, reliable, user-friendly, and compatible with sustainable smart-city energy strategies.

Wireless power transfer (WPT) has gained substantial attention as a safer, more convenient, and maintenance-free alternative to conventional plug-in charging systems [5], [6]. Recent studies further emphasize that wireless power transfer technologies are rapidly advancing due to improvements in resonant inductive coupling, power electronics, and compensation networks, enabling charging efficiencies approaching

The associate editor coordinating the review of this manuscript and approving it for publication was Wei Quan.

or exceeding 90% in modern EV charging systems [7]. Large-scale field demonstrations, including Volvo's wireless EV taxi project in Sweden [8] and in-ground charging infrastructure for buses in Gothenburg [9], confirm its technical maturity and operational feasibility. Unlike wired charging, WPT removes physical connectors, minimizes wear and exposure to harsh environments, improves safety, and enables automated charging, particularly beneficial for fleets, taxis, buses, and shared mobility applications where frequent charging is required [10], [11], [12], [13]. When powered by renewable energy, wireless charging can further reduce dependence on fossil-based grids, improve sustainability, and support decarbonized transport infrastructures [14].

Among renewable sources, photovoltaic (PV) systems are highly attractive due to declining costs, scalability, and rapid global deployment. With appropriate maximum power point tracking (MPPT) strategies such as Perturb and Observe (P&O), PV systems maintain efficient operation under changing environmental conditions [8], while battery storage enables continuous charging during low irradiance periods [9]. Although PV performance may be influenced by dust, shading, and maintenance factors [15], global installed PV capacity exceeding 1.6 TW in 2025 demonstrates its technological maturity and readiness for integration with EV charging infrastructure [16]. Moreover, PV-powered charging can reduce peak-hour grid stress [17] and long-term charging costs, contributing to resilient and cost-effective smart-city energy management frameworks [18], [19], [20]. Beyond metropolitan environments, renewable-powered EV charging is increasingly relevant to public transport applications, service-based mobility, and regions with strong tourism sectors, where decentralized and sustainable charging infrastructure enhances environmental performance and energy resilience [18].

A. EXISTING RESEARCH AND REMAINING CHALLENGES

Although numerous studies have investigated PV-powered EV charging and wireless charging technologies, most existing works:

- primarily consider grid-assisted or single-phase architectures
- do not present fully integrated PV–MPPT–battery–WPT system frameworks
- rarely address multi-phase, multi-vehicle, and dynamic charging scenarios
- provide limited system-level evaluation linking technical performance, efficiency, economic feasibility, and smart-city applicability.

These limitations highlight the need for a comprehensive renewable-powered wireless charging framework capable of supporting both static and dynamic EV charging within smart-city environments

B. OBJECTIVES AND CONTRIBUTION

Motivated by these gaps, this study proposes a fully renewable, PV-integrated wireless charging system (WCS) for electric vehicles, developed and validated through MATLAB/Simulink simulations. The main contributions are:

1) Development of a comprehensive PV–battery–MPPT–SS WPT framework integrating bidirectional DC–DC storage management and inverter-based power conditioning.
2) Design of two configurations:
   - a three-phase static fast-charging system for single-vehicle applications
   - a three-phase system supporting stationary and dynamic multi-vehicle charging modes.
3) Detailed performance evaluation includes DC-link regulation, wireless transfer characteristics, coil-to-coil efficiency, and overall end-to-end efficiency.
4) A techno-economic and smart-city-oriented assessment demonstrating reduced grid dependency, decreased charging cost, and strong suitability for sustainable urban mobility infrastructures.

The primary objective is to design a renewable-powered wireless EV charging solution that advances smart city sustainability goals and reduces (CO_2) emissions. Additionally, the system aims to relieve electricity distribution networks by shifting charging demand to solar energy. This approach contributes to both sustainable mobility and the development of resilient, renewable-powered smart distribution systems for future urban environments.

II. LITERATURE REVIEW

Electric vehicles (EVs) have become central to sustainable mobility by reducing greenhouse gas emissions and lowering dependence on fossil fuels. As EV penetration increases, however, new challenges arise related to charging infrastructure capacity, grid stability, power quality, and long-term energy sustainability. Recent survey studies highlight that wireless EV charging systems are evolving toward higher efficiency, improved coil alignment tolerance, and scalable dynamic charging infrastructure for future smart transportation systems [21]. In response, research has increasingly focused on wireless power transfer (WPT) technologies and renewable-powered charging systems that aim to combine operational convenience with environmental benefits [5], [6], [10], [13]. The integration of photovoltaic (PV) generation with WPT has been viewed as a promising pathway toward decentralized and low-carbon charging infrastructures aligned with smart-city objectives.

Several studies have examined PV-fed EV charging configurations. Partha et al. proposed a grid-connected solar-powered WPT system for EV charging [17], while other researchers developed stand-alone PV-based charging systems capable of directly supplying EV batteries without grid support [22], [23], [24], [25], [26]. These works demonstrate the feasibility of renewable-assisted EV charging; however, many reported implementations operate at relatively modest power ratings and are primarily designed for static charging conditions. In addition, renewable generation is often

treated as a supplementary energy source rather than as a fully coordinated primary supply integrated with storage and dynamic charging control [27]. As a result, the interaction between PV generation, MPPT control, battery buffering, and high-frequency WPT subsystems has not been extensively evaluated within unified system-level architectures.

Wireless EV charging technologies have evolved significantly since early magnetic-resonance demonstrations at MIT, which achieved 60 W power transfer over a 2 m distance [28]. Subsequent developments improved efficiency and scalability, reporting efficiencies between 70% and 96% depending on coil separation, alignment, and compensation topology [29], [30]. High-power laboratory prototypes, such as the 8 kW system developed at the University of Michigan–Dearborn, achieved efficiencies above 95% under controlled conditions [31]. Field implementations, including Bombardier's PRIMOVE system and wireless EV charging trials in Sweden and Gothenburg, have demonstrated operational feasibility in urban transportation environments [19], [20], [32]. These studies confirm the technical maturity of WPT while also highlighting challenges associated with misalignment, dynamic coupling variation, and power regulation.

Among the four primary compensation topologies—series–series (SS), series–parallel (SP), parallel–series (PS), and parallel–parallel (PP)—the SS configuration has consistently demonstrated favorable impedance characteristics and high power transfer efficiency [33], frequently exceeding 90% in EV charging applications [5], [34], [35]. Recent investigations also explore hybrid compensation networks and intelligent control strategies to enhance power transfer efficiency and misalignment tolerance in EV wireless charging systems [36]. Hybrid configurations such as LCL and LCC networks have also been investigated to enhance reactive power control and misalignment tolerance [34], [35], [36]. Nevertheless, the majority of prior work has concentrated on either single-phase or grid-tied implementations [37], [38], with comparatively limited emphasis on multi-phase wireless charging architectures or coordinated renewable-fed dynamic systems.

Control strategies for WPT systems typically rely on voltage- or current-mode regulation using PI-based controllers, impedance-matching techniques, or frequency tuning approaches to maintain resonance and stable power transfer [10], [12]. Recent literature has further explored IoT-enabled monitoring, GaN-based high-frequency converters, and smart-grid-interactive control strategies to enhance efficiency and electromagnetic compatibility [10], [12], [19], [39]. While these contributions advance subsystem performance, many reported designs remain predominantly technology-focused, addressing compensation or converter optimization independently rather than integrating renewable generation, bidirectional storage, and dynamic multi-phase charging within a single coordinated framework.

From a broader infrastructure perspective, renewable-powered EV charging has been studied in the context of distributed energy resources (DERs) and smart-grid integration [11], [13], [14]. Techno-economic analyses demonstrate that PV-based charging can reduce operational costs compared to grid-dependent models [18], [19], [40]. In addition to metropolitan deployments, renewable-integrated charging solutions have been investigated for tourism-driven regions, hospitality infrastructure, and remote destinations, where decentralized, low-maintenance systems offer strategic advantages [41], [42], [43]. These studies underscore the societal relevance of renewable-assisted EV charging while also indicating the need for technically robust, scalable architectures capable of coordinating PV generation, energy storage, and high-power wireless transfer under practical operating conditions. Collectively, the existing literature provides significant advances in compensation topology optimization, magnetic coupling analysis, converter design, and renewable-assisted charging concepts. However, many reported systems remain component-focused, grid-dependent, or limited to static single-phase implementations. Comprehensive system-level architectures that simultaneously coordinate PV generation, MPPT control, bidirectional battery management, multi-phase inverter interfacing, and dynamic wireless charging remain comparatively less explored in the reported body of research.

III. IDENTIFIED RESEARCH GAPS AND NOVELTY POSITIONING

A. RESEARCH GAPS IN RENEWABLE-INTEGRATED DYNAMIC WIRELESS POWER TRANSFER SYSTEMS

Dynamic Wireless Power Transfer (DWPT) has emerged as a promising technology for electrified transportation, particularly for in-motion charging of electric vehicles (EVs). Although substantial research has been conducted on DWPT systems [10], [29], [32], recent studies further highlight the growing importance of DWPT for enabling continuous charging and reducing battery capacity requirements in next-generation EV infrastructures [44].

1) GRID DEPENDENCY AND LACK OF RENEWABLE AUTONOMY

Most reported DWPT implementations are primarily grid-assisted architectures [13], [31], [39], where renewable generation, if present, plays only a supplementary role. These systems:

- Depend heavily on utility grid stability,
- Do not ensure renewable self-sufficiency,
- Lack autonomous operation during grid contingencies.

Even in advanced prototype implementations and field trials [19], [20], [31], grid supply remains the dominant primary energy source. Consequently, the true potential of DWPT as a decentralized, renewable-powered infrastructure remains underexplored in comparison to grid-dependent models [11], [13].

2) LIMITED SYSTEM-LEVEL INTEGRATION

Existing studies predominantly focus on component-level optimization, including:

- Compensation topology design [33], [36], [37], [38],
- Magnetic coupling variation analysis [29], [34],
- Control strategy enhancement [11], [13],
- Power electronics converter optimization [41], [45].

While these contributions are technically valuable, they typically isolate subsystems rather than presenting a fully integrated energy architecture. Very few works simultaneously incorporate:

- Photovoltaic (PV) generation [17], [22], [23], [24], [25], [26],
- Maximum Power Point Tracking (MPPT) [27],
- Bidirectional battery energy storage,
- Three-phase inverter interfacing,
- Series–Series (SS) compensated dynamic WPT [33], [37].

In most reported implementations, renewable generation and energy storage are either absent or loosely coupled to the WPT stage [26], [40]. The absence of such integrated frameworks limits practical deployment and scalability under realistic operating conditions.

3) SCARCITY OF MULTI-PHASE RENEWABLE-FED DWPT IMPLEMENTATIONS

Most published DWPT prototypes are:

- Single-phase systems [39], [40],
- Grid-fed architectures [13], [31],
- Without coordinated battery buffering [26],
- Limited to laboratory-scale demonstrations [31], [36].

Although multi-phase power conversion is widely adopted in conventional charging infrastructures, its coordinated integration with renewable-fed DWPT architecture remains scarcely reported. Configurations that simultaneously coordinate PV generation, energy storage, and dynamic charging under realistic operating scenarios are comparatively limited in the reported literature.

4) INSUFFICIENT SMART-CITY AND DER PERSPECTIVE

Despite the relevance of DWPT to sustainable urban mobility, existing research rarely evaluates:

- End-to-end renewable efficiency [17],
- Grid stress mitigation potential [11], [13],
- Distributed Energy Resource (DER) compatibility [14],
- Comparative charging cost versus grid electricity [18], [19], [43],
- System behavior under fluctuating renewable generation.

While techno-economic analyses have been performed for PV-based EV charging infrastructures [18], [19], [43], most wireless charging studies remain technology-centric, focusing on electromagnetic or converter-level performance rather than infrastructure-oriented deployment perspectives. Thus, DWPT research remains largely component-driven rather than infrastructure-centric

B. DISTINCTION FROM PRIOR DYNAMIC WPT WORKS

Unlike the majority of previously reported dynamic wireless power transfer (DWPT) studies, which concentrate primarily on compensation topology optimization [33], magnetic coupling variation [29], or control enhancement at the subsystem level [11], [13], the present work advances a renewable-integrated, system-oriented DWPT architecture that addresses the entire energy conversion chain from generation to vehicle charging. Rather than treating wireless power transfer as an isolated electromagnetic problem, this research conceptualizes DWPT as a coordinated renewable energy node within a distributed energy ecosystem [14].

The proposed framework integrates a photovoltaic (PV) array equipped with maximum power point tracking (MPPT) [27], bidirectional battery energy storage governed by battery management system (BMS) coordination, a three-phase inverter interface, and a series–series (SS) compensated wireless power transfer structure capable of both static and dynamic operation [33], [37]. This unified architecture ensures that energy production, conversion, buffering, and transfer are cohesively managed within a single renewable-fed platform. Such end-to-end integration is rarely demonstrated in prior literature, where renewable generation and energy storage are often either omitted or loosely coupled to the WPT stage [26], [40].

To demonstrate scalability and practical feasibility, two distinct system configurations are developed and evaluated: a 4 kW architecture representing modular or localized deployment scenarios, and a 31.5 kW high-power configuration suitable for corridor-level or infrastructure-scale implementation. This dual-scaling approach enables performance validation across different power levels while preserving architectural consistency, thereby supporting extensibility in real-world smart-city environments.

A defining characteristic of the proposed system is its renewable autonomy. Unlike grid-assisted DWPT systems [13], [31], the architecture is designed to operate independently of the utility grid, thereby demonstrating a fully renewable-powered charging node. This autonomy enhances energy resilience and reduces dependency on centralized infrastructure, positioning the system as a sustainable alternative for electrified transportation networks.

The inclusion of bidirectional battery storage further strengthens operational stability by mitigating the intermittency inherent in photovoltaic generation [17], [27]. The battery layer provides energy buffering, smooths short-term renewable fluctuations, and ensures stable power delivery during vehicle motion under dynamic charging conditions. As a result, power continuity and charging reliability are improved, particularly under transient or partially shaded PV conditions.

Beyond technical validation, the study extends its scope to charging performance and economic evaluation. Comparative analyses are conducted to assess charging duration and renewable-based cost efficiency relative to conventional

grid electricity pricing [18], [19], [43]. This broader techno-economic perspective distinguishes the present work from topology-centric studies and provides actionable insight for infrastructure planning.

Finally, the proposed architecture is framed within the context of smart-city Distributed Energy Resources (DERs) [11], [13], [14]. By functioning as a modular renewable charging node, the system contributes to grid stress reduction, promotes localized renewable utilization, and supports scalable deployment along urban transportation corridors. Consequently, the novelty of this research resides not merely in compensation design or magnetic optimization, but in the holistic integration of renewable generation, storage coordination, multi-phase conversion, and dynamic wireless charging within a scalable DER-oriented framework suitable for next-generation sustainable mobility infrastructure.

The novelty of this work does not lie solely in compensation topology, mathematics, or magnetic coupling optimization. Instead, it resides in the system-level integration of renewable generation, energy storage, and multi-phase dynamic wireless charging into a scalable and autonomous architecture suitable for smart-city DER deployment. A structured comparative analysis between representative WPT studies and the proposed renewable-integrated configurations is presented in Table 8, highlighting differences in renewable autonomy, phase configuration, dynamic capability, and system-level integration

IV. METHODOLOGY

A. SYSTEM ARCHITECTURE

The proposed system architecture is illustrated in Fig. 1. The framework integrates photovoltaic (PV) panels as the primary renewable energy source and incorporates several essential subsystems, including a DC–DC boost converter for voltage regulation, a DC–AC inverter for grid-compatible conversion, battery storage for energy buffering, and rectification stages for power conditioning. A series–series (SS) compensation topology is implemented within the wireless power transfer (WPT) subsystem to ensure efficient inductive coupling between the transmitting (Tx) and receiving (Rx) coils. Each module has been individually designed, modeled, and validated in MATLAB/Simulink under varying operating conditions to ensure reliability and performance consistency.

From a practical deployment perspective, this architecture is suitable for applications such as high-demand bus depots during peak charging periods and household overnight charging scenarios where renewable availability enhances system sustainability. Fig. 1 demonstrates the structural relationship among the PV source, conversion stages, compensation network, and EV charging interface. The complete energy-conversion architecture of the proposed PV-integrated WCS, highlighting each processing stage, is further presented in Fig. 1.

In addition to functioning as an independent EV charging station, the proposed configuration can operate as a modular unit within smart-city distribution networks. By integrating

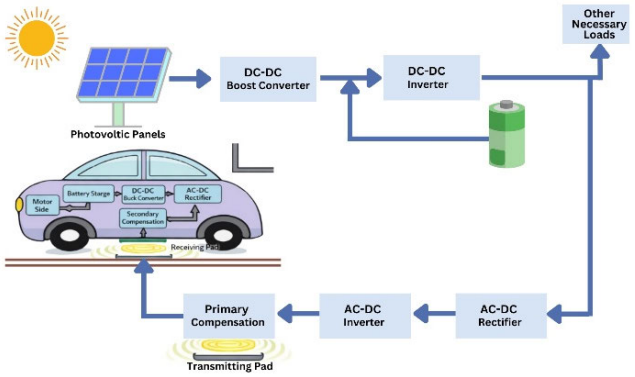

FIGURE 1. System architecture of the suggested system.

PV generation and battery storage, the system reduces grid loading, improves renewable penetration, and supports sustainable urban mobility. In the proposed system, the PV array generates DC power, which is stepped up through a boost converter and subsequently inverted to AC via the PV inverter subsystem. This AC power may either supply local loads or be injected into the grid. Simultaneously, a portion of the regulated AC is rectified by DC on the primary side to energize the WPT subsystem. The overall power-transfer chain can be summarized as:

PV → Boost Converter (DC–DC) → Inverter (DC–AC for local use) → Rectifier (AC–DC for WCS) → SS-Compensated WPT Network → Secondary Rectifier (AC–DC) → Buck Converter → EV DC link.

B. OPERATIONAL FLOW

The operational sequence of the proposed charging framework is presented in Fig. 2. The process begins with PV panels generating DC electricity, which is conditioned through a DC–DC boost converter to maintain the required operating voltage. The regulated DC is subsequently converted into AC via an inverter to feed the inductive power transfer system. A battery storage unit is integrated to enhance system flexibility and resilience. During peak irradiance, surplus solar energy is stored in the battery, while during low-irradiance conditions, the stored energy supports uninterrupted EV charging. When storage is unnecessary, harvested solar power is supplied directly to the inverter, achieving a seamless ''sun-to-wheel'' charging pathway. This arrangement ensures continuous, stable, and reliable wireless charging. From a smart-city perspective, this operational structure provides dual advantages: (i) enabling renewable-powered wireless charging and (ii) alleviating stress on urban distribution networks by shifting charging demand toward locally generated solar energy and stored capacity. Fig. 2 summarizes the sequential control and energy-flow pathway from PV generation to EV charging.

C. FUNCTIONAL PATTERN

The proposed system consists of two principal subsystems: the power-supply unit and the wireless charging system

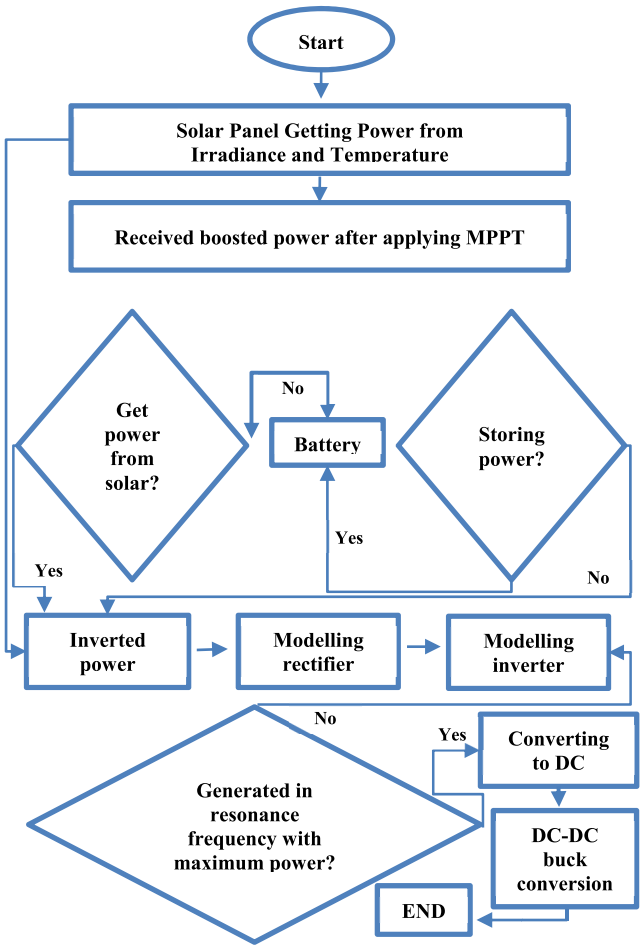

FIGURE 2. Operational flow of the proposed system.

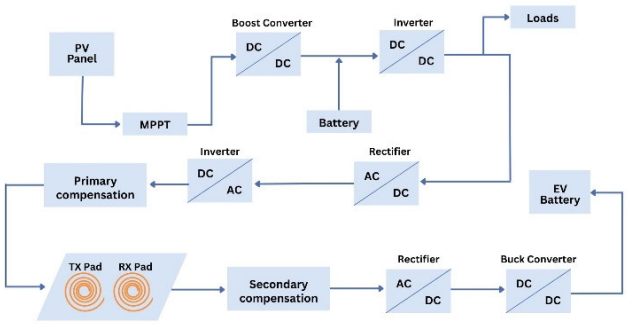

FIGURE 3. Functional Pattern of the suggested system.

TABLE 1. System parameters for wireless charging models.

Parameters	Design value
L_1 and L_2	200 µH
C_1 and C_2	17.9 nF
R_1 and R_2	1 Ω
M	40 µH
Filter 1 and Filter 2	100 µH
Co-efficient, k	0.2

The parameters include the self-inductances (L_1, L_2), capacitances (C_1, C_2), and resistances (R_1, R_2) of the primary and secondary coils, as well as the mutual inductance (M) and coupling coefficient (k). The filter inductances are selected to minimize current ripple and maintain stable resonance at the designed operating frequency.

(WCS), as shown in Fig. 3. The power-supply side comprises a PV array equipped with MPPT control, a boost converter, and a PV inverter stage. The WCS consists of primary-side compensation driven by an inverter and secondary-side compensation followed by a rectifier to supply the EV load. To ensure maximum power transfer, the system operates at the resonant frequency. The SS compensation arrangement establishes the resonance condition as

$$f_0 = \frac{\omega_0}{2\Pi} = \frac{1}{2\Pi\sqrt{L_1C_1}} = \frac{1}{2\Pi\sqrt{L_2C_2}} \tag{1}$$

where $L_1 = L_2$ and $C_1 = C_2$ are the self-inductance and self-capacitance of the transmission and receiving coil. The coefficient of magnetic coupling is determined

$$k = \frac{M}{\sqrt{L_1L_2}} \tag{2}$$

In equation (2), M is the mutual inductance, and Tx and Rx are the Tx and Rx coils. Initially, coil parameters are simulated to evaluate efficiency performance. Using (1) and (2), the system design parameters are calculated and summarized in Table 1. The resulting resonant frequency is approximately 84.2 kHz, which aligns closely with the standard 85 kHz operating frequency specified by SAE J2954 for EV-WPT applications. Table 1 lists the final design parameters for the proposed WCS models, including inductances, capacitances, resistances, mutual inductance, and coupling coefficient. Filter inductances are selected to minimize current ripple and maintain stable resonance at the designed frequency.

D. COIL DESIGN AND PARAMETER DERIVATION

To strengthen the engineering foundation of the wireless power transfer subsystem, the coil parameters listed in Table 1 are derived based on resonance requirements and practical EV charging constraints rather than arbitrary selection.

From the resonance condition defined in (1), the operating frequency is determined by the self-inductance and compensation capacitance. Since the target operating frequency is approximately 85 kHz in accordance with SAE J2954 guidelines, the inductance–capacitance pair must satisfy equation (1). By selecting a practical inductance value suitable for mid-power EV wireless charging applications, $L_1 = L_2 = 200\mu$H, the corresponding compensation capacitance calculated from (1) yields approximately $C_1 = C_2 = 17.9$nF, ensuring resonance near 84.2 kHz.

1) INDUCTANCE SELECTION AND COIL GEOMETRY CONSIDERATIONS

The inductance value of 200 μH was chosen based on practical circular planar coil configurations commonly adopted in EV wireless charging systems. For an air-core circular spiral coil, the inductance can be approximated using:

$$L \approx \frac{\mu_0 N^2 r^2}{8r + 11w} \tag{3}$$

where, N = number of turns, r = average radius of the coil, w = winding width, and μ_0 = permeability of free space. Using realistic EV underbody constraints (typical coil outer diameter in the range of 40–50 cm and air gap between 150–200 mm), the selected inductance value of 200 μH represents a practical and achievable design point for mid-range dynamic charging systems. This inductance range is consistent with reported EV WPT implementations operating near 85 kHz [33], [37] while recent studies also demonstrate that optimized coil geometry and resonant coupling significantly improve wireless power transfer efficiency and stability in EV charging applications [46].

2) MUTUAL INDUCTANCE AND COUPLING COEFFICIENT DERIVATION

The magnetic coupling coefficient defined in (2) relates mutual inductance to self-inductances. For symmetric coils where $L_1 = L_2 = 200\mu$H,the mutual inductance becomes:

$$M = k\sqrt{L_1 L_2} \tag{4}$$

A nominal coupling coefficient of $k = 0.2$ was selected to represent realistic mid-range alignment conditions in dynamic EV charging. Under the condition of M= 0.2×200 μH=40 μH, this value reflects moderate coupling typical of practical EV air-gap separations and alignment tolerances reported in dynamic WPT studies [29], [33]. The selection of $k = 0.2$ ensures stable power transfer under non-ideal alignment while avoiding optimistic coupling assumptions

3) DYNAMIC OPERATION CONSIDERATIONS

In dynamic wireless charging scenarios, the coupling coefficient varies due to vehicle motion and lateral misalignment. Practical DWPT systems typically operate within a coupling range of 0.15–0.3, depending on alignment and air gap [27], [31]. The selected design point, therefore, represents a conservative mid-range condition suitable for both static and dynamic operation modes.

The SS compensation topology was retained due to its favorable impedance behavior and robustness under moderate coupling variation [33], [37], ensuring stable resonant operation despite dynamic changes in magnetic linkage.

4) LOSS MODELING AND PRACTICAL ASSUMPTIONS

To account for high-frequency effects at 85 kHz, winding resistances R_1 and R_2 were modeled as 1 Ω, representing copper losses and parasitic effects under practical litz-wire implementation. Filter inductances were included to suppress current ripple and maintain DC-link stability under switching operation. The resulting coil-to-coil efficiency of approximately 91.7% validates that the selected inductance, coupling coefficient, and compensation values provide high transfer efficiency while remaining within practical EV charging constraints.

E. CONTROL STRATEGY AND IMPLEMENTATION

The proposed renewable-integrated wireless charging system employs a hierarchical control architecture consisting of three coordinated control layers: (i) PV-side MPPT control, (ii) DC-link voltage regulation, and (iii) wireless power transfer regulation.

1) PV-SIDE MPPT AND BOOST CONVERTER CONTROL

The photovoltaic subsystem operates under a Perturb and Observe (P&O) Maximum Power Point Tracking (MPPT) algorithm to ensure optimal energy extraction under varying irradiance conditions [27]. The MPPT block dynamically adjusts the duty cycle of the DC–DC boost converter to maintain operation at the maximum power point. The boost converter regulates the PV output voltage to match the required DC-link level while compensating for solar variability.

2) DC-LINK VOLTAGE REGULATION

To ensure stable operation of the inverter and WPT subsystem, the DC-link voltage is maintained at a predefined reference level using a closed-loop voltage control strategy. A PI controller regulates the inverter modulation index to maintain DC-link stability. This stage ensures that fluctuations from the PV array or battery do not destabilize the high-frequency WPT inverter.

3) WIRELESS POWER TRANSFER REGULATION

The WPT inverter operates at a fixed switching frequency close to the resonant frequency (≈85 kHz) determined by Eq. (1). Maintaining a constant switching frequency preserves the resonance condition of the SS-compensated network under nominal coupling conditions. Power regulation is implemented using a voltage-mode control strategy on the primary side. Specifically, the transmitted power is controlled by adjusting the inverter excitation level (i.e., modulation index or duty ratio), which effectively regulates the input voltage applied to the resonant tank. By modulating the inverter output amplitude rather than varying the switching frequency, the system maintains stable resonant operation while controlling the magnitude of transferred power. This approach ensures that resonance is not disturbed during regulation and enhances stability under moderate coupling variations encountered in practical static and dynamic charging scenarios.

4) SECONDARY-SIDE RECTIFIER AND BUCK CONTROL

On the receiver side, the rectified DC output is regulated through a buck converter operating under closed-loop current

control. The EV charging current is maintained at the desired reference value according to battery charging requirements. A PI-based current controller adjusts the duty cycle of the buck converter to regulate charging power and prevent over-current conditions.

5) BATTERY ENERGY MANAGEMENT

The integrated battery storage subsystem operates under bidirectional DC–DC control. During excess PV generation, the battery absorbs surplus energy, while under low-irradiance conditions, it supplies energy to maintain uninterrupted charging. The battery management logic ensures:

- Voltage protection
- State-of-charge monitoring
- Seamless transition between charging and discharging modes

This coordinated control framework enables renewable autonomy while ensuring stable and efficient wireless charging.

F. PRACTICAL SYSTEM INTERCONNECTION AND OPERATIONAL MODES

Although Figs. 1–3 illustrate the structural arrangement of subsystems, and the practical electrical interconnection and operational coordination are clarified as follows. The PV array feeds a DC–DC boost converter, which regulates the PV voltage under MPPT control. The boosted DC output is connected to a common DC-link bus. This DC-link serves as the central energy node of the system and interfaces with:

1) The primary-side high-frequency inverter of the WPT subsystem,
2) The bidirectional battery converter,
3) The grid-interfacing inverter (if grid-connected mode is enabled).

Under normal high-irradiance conditions, the PV array supplies the DC-link directly. Surplus energy is routed to the battery through the bidirectional DC–DC converter when the DC-link voltage exceeds its reference threshold. Conversely, during low-irradiance or transient conditions, the battery discharges to maintain DC-link stability and ensure uninterrupted wireless power transfer. The primary-side inverter converts the regulated DC-link voltage into high-frequency AC excitation for the SS-compensated resonant tank. The transmitter coil generates an alternating magnetic field, inducing an AC voltage in the receiver coil. On the secondary side, a rectifier converts the induced AC into DC, which is subsequently regulated by a buck converter before being delivered to the EV DC link.

System operation can be categorized into three principal modes:

- PV power directly feeds the WPT subsystem when generation is sufficient.
- PV and battery jointly maintain DC-link stability during fluctuating irradiance or dynamic coupling variation.
- Battery exclusively supplies the WPT subsystem during low or zero solar conditions.

These coordinated operating modes ensure continuous power delivery to the EV while maintaining DC-link stability and protecting subsystem limits. The centralized DC-link architecture simplifies power routing and enables seamless transitions between renewable generation and stored energy support.

V. SIMULATION MODEL DESIGNING AND STRUCTURING

This research focuses on integrating photovoltaic (PV) generation with maximum power point tracking (MPPT) for wireless power transfer (WPT) in electric vehicles (EVs). To validate the concept, two distinct models of PV-integrated wireless charging systems (WCS) have been developed:

a) PV-integrated three-phase fast charging system for static single-vehicle charging (Proposed Model I)

b) PV-integrated three-phase system for stationary and dynamic multiple-vehicle charging modes (Proposed Model II)

Both models share common subsystems—including PV generation, MPPT, power conditioning, and compensation circuits—and therefore, identical subsystem figures and descriptions are not repeated. Instead, emphasis is placed on system parameters, simulation models, and power electronic configurations that differentiate the two proposed designs. From a smart city perspective, Proposed Model I is particularly suited for residential or small-scale charging points, while Proposed Model II offers scalability for public transport hubs, parking facilities, and dynamic charging lanes. Together, these models demonstrate how PV-integrated WCS can be adapted to diverse urban contexts, supporting sustainable mobility while reducing pressure on distribution grids through renewable-based charging.

A. PROPOSED SIMULATION MODEL

It is perceived that the proposed system comprises several subsystems, as shown in Fig. 5 and Fig. 6. The PV inversion subsystem receives power from the PV system. After that, the power is inverted to the primary side, and the remaining power is supplied to other necessary loads. Then, the power is rectified to the primary-side inverter subsystem for transferring it to the secondary side using a compensation topology. On the secondary side, the rectifier subsystem rectifies the transferred power. A DC-DC buck converter subsystem is connected to the rectifier subsystem to feed steady power. The detailed simulation architectures of Models I and II are presented in Figs. 5 and 6, respectively, showing the subsystem interconnections.

B. PV SYSTEM WITH MPPT SUBSYSTEM

In Fig. 6, a PV with an MPPT subsystem is shown. For the WPT system, this paper considers a PV with an MPPT system, a boost converter, and a battery to maximize power transfer to the PV inversion subsystem. The schematic

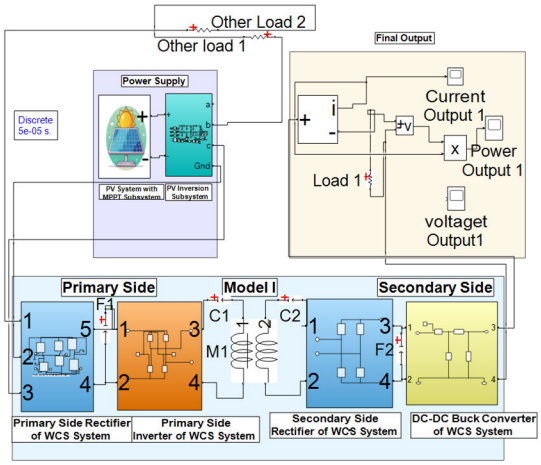

FIGURE 4. Simulation architect of Proposed Model I.

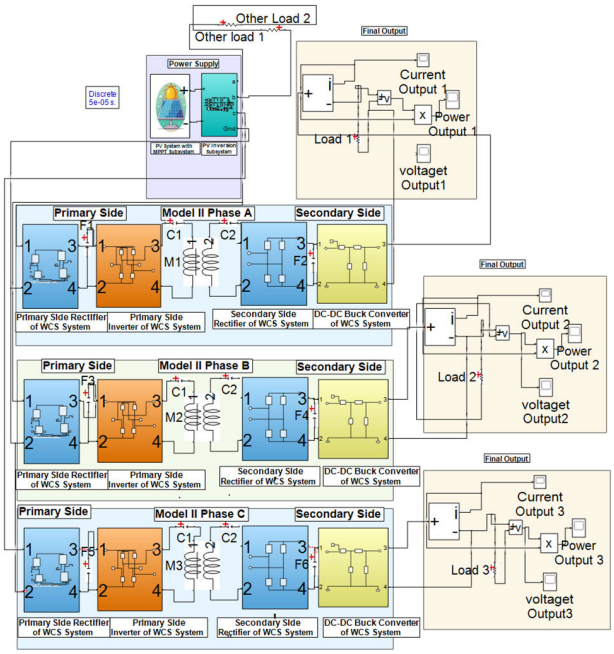

FIGURE 5. Simulation architect of Proposed Model II.

representation of the photovoltaic subsystem with MPPT control is shown in Fig. 6

However, two PV systems are designed for this proposed research work. A 4.8 kW rated PV system is assigned for Model I, and a 35.5 kW rated PV system is appointed for Model II. The PV module characteristics and required parameters are shown in Table 2.

1) BOOST CONVERTER

A boost converter is used in this subsystem for stepping up the power to the load. For designing the boost converter, an IGBT/Diode is used for switching, and to construct the

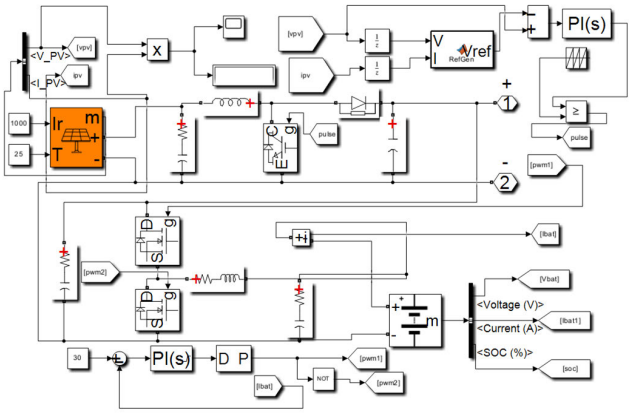

FIGURE 6. PV with MPPT subsystem.

TABLE 2. PV module characteristics and required parameters.

Parameters	Values for a 4.8 kW rated PV system for Static Mode (Model I)	Values for a 35.5 kW-rated PV system for Stationary and Dynamic Mode (Model II)
Maximum Power (W)	213.5	213.5
Open Circuit Voltage Voc (V)	36.3	36.3
Vmp (V)	29	29
Voc (%/deg.C)	-0.36	-0.36
Current at maximum power point Imp (A)	7.38	7.38
Series Modules	21	21
Parallel Strings	1	8

Each PV module is rated at 213.5 W (Voc = 36.3 V, Vmp = 29 V, Imp = 7.38 A). Model I uses 21 series-connected modules (≈4.8 kW), while Model II consists of 21 modules per string with eight parallel strings (≈35.5 kW), ensuring the required DC-link voltage and balanced power delivery.

boost converter, parameters are calculated using the equations below [47]:

$$L = \frac{V_{ip}(V_{op} - V_{ip})}{f_{sw} * \Delta I * V_{op}} \tag{5}$$

$$C = \frac{I_{op}(V_{op} - V_{ip})}{f_{sw} * \Delta V * V_{op}} \tag{6}$$

2) P&O ALGORITHM

The most applicable method is perturbed and observed (P&O), which is applied to the PV system in this paper.

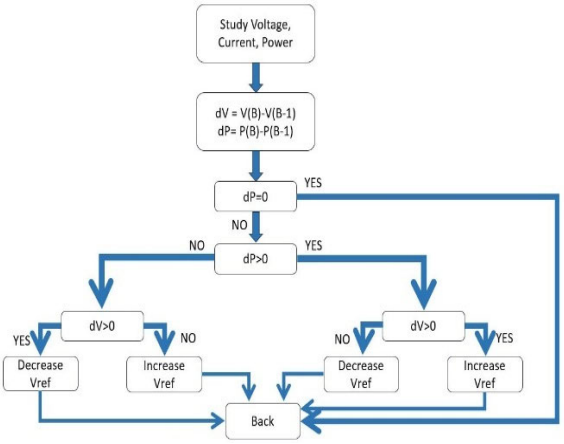

FIGURE 7. Process of P&O MPPT Technique.

This subsystem is simulated in some steps. The algorithm's process is shown in Fig. 7.

- Step 1: Measuring the voltage and current values from the PV panel
- Step 2: Calculating the PV power
- Step 3: Checking the differentiation in power and voltage
- Step 4: If variation in voltage is increasing and power is positive, or voltage is decreasing, and power is negative, then the duty cycle will be:

$$\mathrm{d}_{n-1}\,(previous\ Value) + \delta or \mathrm{d}_{n-1}\,(previous\ Value) - \delta \quad (7)$$

At the static state, the duty cycle is 0.5, but when irradiance changes, the power changes as well, so the duty cycle adjusts accordingly.

3) BATTERY WITH DC-DC BIDIRECTIONAL CONVERTER

One battery is used in this subsystem for later use if the consumer needs electricity or power is unavailable. This model is aligned with charging and discharging modes. However, the converter is in continuous mode, with two MOSFETs used as active devices and diodes. When MOSFET S_1 is active, the converter works in boost operational mode, and MOSFET S_2 acts as a diode. Other results occur when the situation is contrary. Despite that, the converter is designed using these equations:

$$L = \frac{(V_{out}(V_{in} - V_{out}))}{(V_{ripple} * fsw * V_{in})} \quad (8)$$

$$\boldsymbol{C} = \frac{\boldsymbol{I}_{ripple}}{(8fsw * \boldsymbol{V}_{ripple})} \quad (9)$$

The parameters of the battery and bidirectional DC-DC converter are shown in Table 3.

4) BATTERY MANAGEMENT SYSTEM (BMS)

The Battery Management System (BMS) serves as a supervisory control layer in the proposed PV–battery–wireless charging architecture, ensuring safe operation, coordinated energy management, and enhanced battery lifetime, as illustrated in Fig. 8. The BMS continuously acquires voltage, current, and auxiliary measurement signals from the battery pack and performs key internal functions including State-of-Charge (SOC) estimation, protection logic, cell-balancing control, and decision-making. SOC estimation is achieved using measured current and voltage feedback supported by coulomb-counting principles, enabling the BMS to determine appropriate charging and discharging actions. Based on this assessment, the BMS communicates bidirectional control commands—such as charge, discharge, current limitation, and protection signals—to the DC–DC bidirectional converter. During periods of high solar availability, surplus PV energy is directed to controlled battery charging, while under low irradiance or transient load conditions, the battery is allowed to discharge in a regulated manner to stabilize the DC link and maintain uninterrupted EV charging. Protection mechanisms against over-voltage, under-voltage, over-current, short-circuit, and abnormal temperature conditions are embedded to ensure operational safety. In addition, balancing control equalizes cell voltages, reducing uneven

TABLE 3. Parameters of battery and bidirectional dc-dc converter.

Parameter	Value
Switching Frequency	5 kHz
Converter Type	DC–DC Bidirectional (Boost/Buck Modes)
Semiconductor Devices	2 × MOSFETs + Diodes
Battery Type	Lithium-ion
Nominal Voltage	360 V
Rated Capacity	150 Ah
Nominal Energy	54 kWh
Initial State-of-Charge (SOC)	50 %

With a switching frequency of 5 kHz, the bidirectional DC–DC converter enables efficient energy management in both charging and discharging modes. With a 360 V and 150 Ah (approximately 54 kWh) rating and an initial state-of-charge (SOC) of 50%, the lithium-ion battery pack ensures balanced operation throughout the simulation period. The model is proportionately scaled to sub-kilowatt levels in MATLAB/Simulink to enhance numerical stability while precisely maintaining the charge–discharge dynamics and control behavior, even though these parameters match those of a full-scale EV battery.

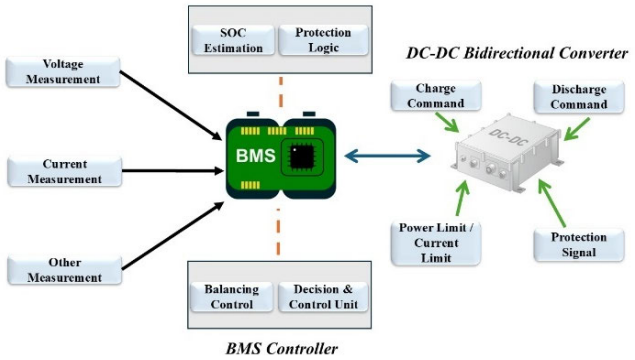

FIGURE 8. Battery management logic for the proposed system.

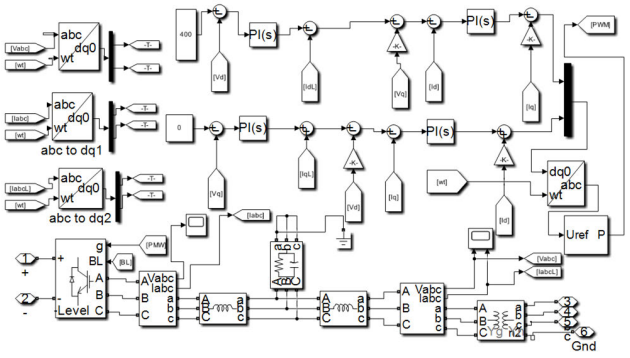

FIGURE 9. PV inversion subsystem of both models.

aging and improving usable capacity. Unlike a basic BMS that only performs passive monitoring, the proposed BMS is tightly integrated into the PV–battery–WPT control loop, enabling coordinated hybrid power operation, ripple suppression, reduced cycling stress, and improved system reliability. This behavior is consistent with the simulation results, where the battery SOC remained close to 70% and residual power imbalance was minimal, confirming stable and practical operation for smart-city, residential, and high-power EV charging applications.

Fig. 8. Conceptual block diagram of the Battery Management System (BMS) integrated with the bidirectional DC–DC converter in the proposed PV–battery–wireless charging system, illustrating measurement inputs, SOC estimation, protection logic, balancing control, and charge–discharge coordination.

C. PV INVERSION SUBSYSTEM

To invert DC power to AC for wireless charging and other loads, an inverter is used in the simulation. This inversion subsystem also includes some operational steps. Firstly, sensing the voltage and current on the load side and converting them to direct and quadrature coordinates. After that, it is applied to the PI controller, and the signals are applied to the pulse via modulators using a transformation block, as shown in Fig. 8. Fig. 8 illustrates the PV inversion subsystem and the associated control strategy used in both models.

For calculating the filter's values, some equations are used:

$$I_o = \frac{P_o}{V_o} \tag{10}$$

$$L = \frac{V_{dc}}{4 * f_{sw} * \Delta I_{ppmax}} \tag{11}$$

$$C = \left(\frac{10}{2 * \pi * f_{sw}}\right)^2 * \frac{1}{L} \tag{12}$$

and for the inverter controller (voltage loop and current loop), other equations are used, which are listed below:

$$K_p = {}^{C}/_{T} \tag{13}$$

$$K_c = {}^{R_c}/_{T} (14) \tag{14}$$

D. PRIMARY SIDE RECTIFIER OF WIRELESS CHARGING SYSTEM

In this suggested system, the regulated DC power from the PV inverter stage is converted to high-frequency AC for the wireless power transfer (WPT) transmitter coil by a primary-side inverter. To create the magnetic coupling between the primary and secondary coils, the inverter stage stimulates the Series–Series (SS) compensated network. The received AC is subsequently transformed back into DC for the EV DC link by a secondary-side rectifier on the receiver side. The inverter and rectifier subsystems utilized in this design are depicted in Fig. 9. Fig. 9 shows the subsystem's model. The controlled rectifier provides uninterrupted power to the rest of the system. For triggering the detailed thyristor, the pulse generator is used using the equations below [47]:

$$Period = \frac{T}{F} \tag{15}$$

$$\textbf{\textit{Phase delay}} = \frac{\boldsymbol{T * Fireangle}}{\mathbf{360^\circ}} \tag{16}$$

E. PRIMARY SIDE INVERTER OF WIRELESS CHARGING SYSTEM

The DC/AC Inverter subsystem of this proposed system is shown on Fig. 10. A full-bridge inverter with IGBTs and four gate pulses for its operation is designed. The DC power from PV is transferred to the secondary side. The detailed subsystem configuration of the wireless charging stages, including the inverter, rectifier, and buck converter, is presented in Fig. 10

F. SECONDARY SIDE RECTIFIER OF WIRELESS CHARGING SYSTEM

The AC/DC rectifier subsystem of this proposed system is shown on Fig. 10. This rectifier rectifies the transferred AC voltage from the primary side of the WCS system.

G. DC-DC BUCK CONVERTER OF WIRELESS CHARGING SYSTEM

A DC-DC buck converter for WCS is designed for this proposed work, as shown in Fig. 10. The DC-DC buck converter

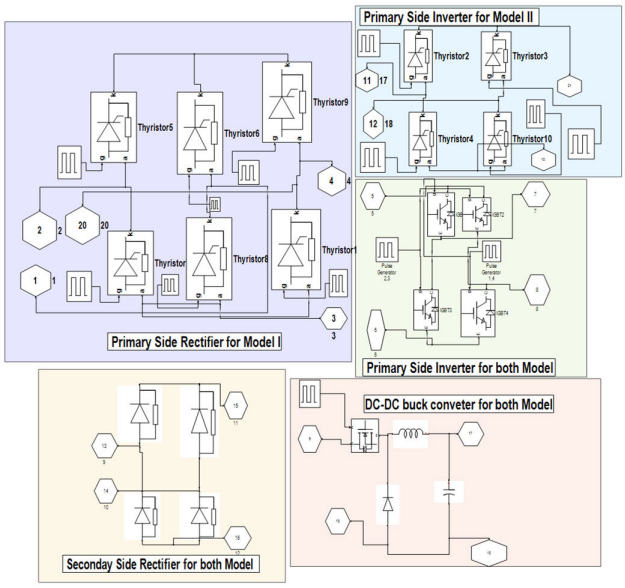

FIGURE 10. Primary side rectifier, inverter, and secondary side rectifier, DC-DC buck converter of the WCS system.

steps down the rectified power and delivers a steady power to the charging section. This subsystem is designed with some equations below [11]:

$$v_0 = v_{in} \times D \tag{17}$$

$$i_R = \frac{v_0}{R_L} \tag{18}$$

$$C = \frac{(1\text{-D})\, v_0}{8Lf^2 \Delta v_0} \tag{19}$$

$$\boldsymbol{L = \frac{(v_{in} - v_0)\, D}{\Delta i_L \times f}} \tag{20}$$

VI. SIMULATION RESULT ANALYSIS

In this proposed system, three kinds of results are observed in the simulation period. These are:

- Simulation result of PV system with MPPT subsystem, PV inversion subsystem, and Battery output result without WCS system for Proposed Model I and Proposed Model II
- Simulation result of three-phase fast charging system for static single-vehicle charging (Proposed Model I) with and without buck converter.
- Simulation result of three-phase system for stationary and dynamic multiple-vehicle charging modes (Proposed Model II) with and without buck converter.

A. PV SYSTEM WITH DIFFERENT MODIFICATIONS

Simulation results of every section are described below:

1) SIMULATION RESULT ANALYSIS OF PV SYSTEM WITH MPPT SUBSYSTEM (MODEL I AND MODEL II)

The PV subsystem was designed separately for both WCS models. For Model I, the boosted PV output stabilizes at approximately 594 V with an output current of ≈7.92 A, delivering ≈4.69 kW, as shown in Fig. 11. For Model II, higher-rated PV capacity enables ≈34.8 kW output with a corresponding current of ≈35.5 A, as presented in Fig. 12.

In both cases, the voltage and power curves show smooth convergence and stable operation, indicating effective MPPT regulation and confirming the PV system's ability to sustain required charging levels under steady-state operation.

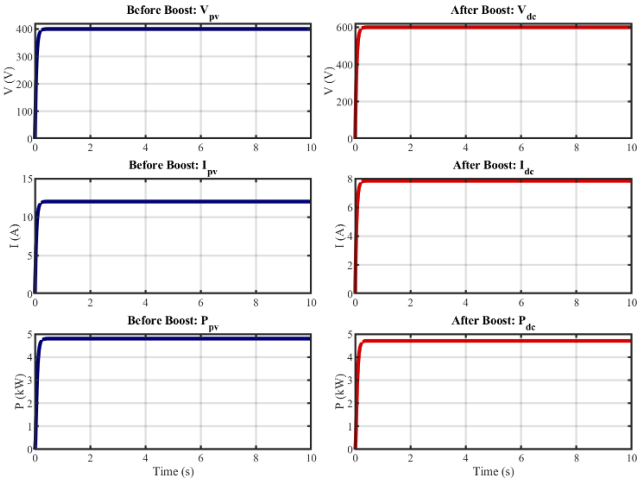

FIGURE 11. Simulation result of PV system for the three-phase fast charging system of static single-vehicle charging (Proposed Model I).

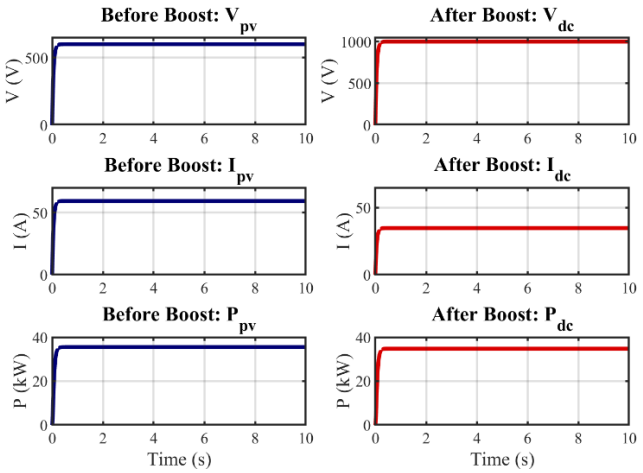

FIGURE 12. Simulation result of PV system for three-phase for stationary and dynamic multiple-vehicle charging modes (Proposed Model II).

2) SIMULATION RESULT ANALYSIS OF PV INVERSION SUBSYSTEM (MODEL I AND MODEL II)

Figs. 13 and 14 illustrate the inverter output waveforms. For Model I, the inverter provides balanced three-phase AC corresponding to an average load power of ≈4 kW, consistent with typical single-vehicle charging requirements (SAE J1772 Level 2 range). For Model II, the inverter supplies ≈33 kW, aligned with multi-vehicle or high-power charging scenarios (SAE J1772 Level 3 range).

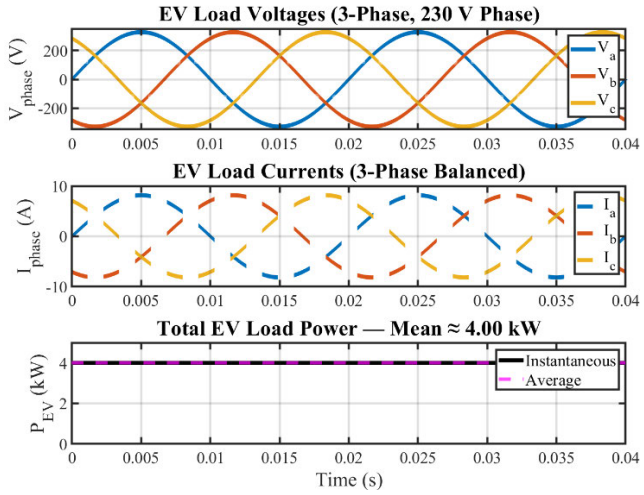

FIGURE 13. Simulation result of PV Inversion for the three-phase fast charging system of static single-vehicle charging (Proposed Model I).

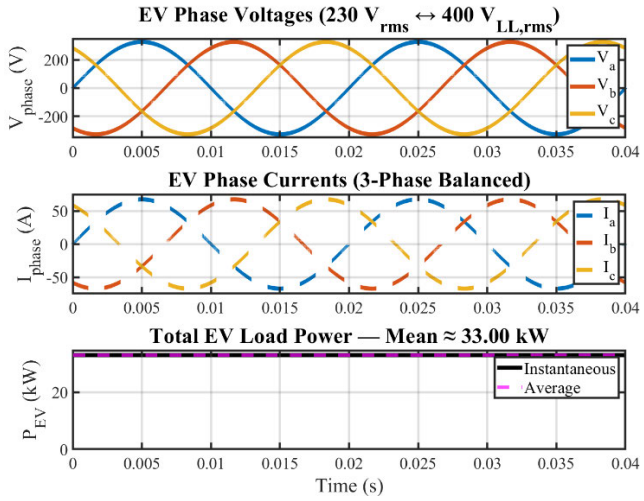

FIGURE 14. Simulation result of PV Inversion for a three-phase system for stationary and dynamic multiple-vehicle charging modes (Proposed Model II).

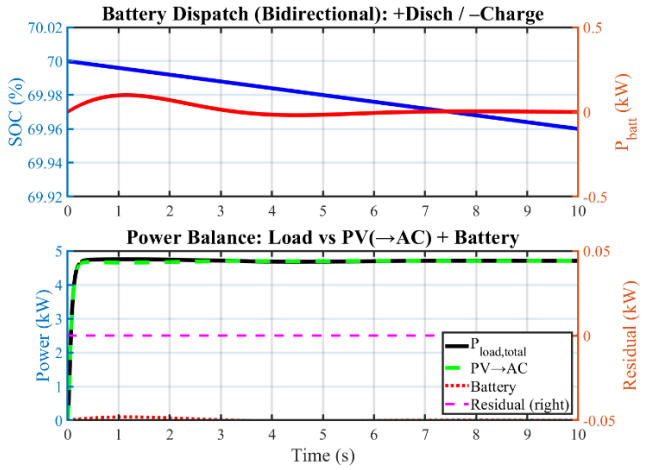

FIGURE 15. Simulation result of the battery in charging and discharging mode for the three-phase fast charging system for static single-vehicle charging, Proposed Model II.

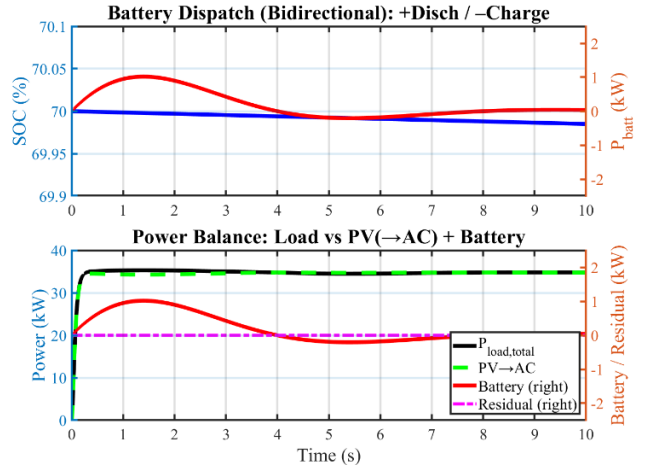

FIGURE 16. Simulation results for the battery in charging and discharging modes for Proposed Model II.

The balanced sinusoidal phase outputs demonstrate correct inverter synchronization, proper DC-link support, and stable grid-compatible AC generation without noticeable distortion, validating power-quality suitability for WPT operation.

3) SIMULATION RESULT OF BATTERY WITH BIDIRECTIONAL DC-DC BOOST CONVERTER

Fig.15 shows the battery dispatch and power balance of the hybrid PV–battery system. The top plot illustrates the battery's bidirectional behavior, where it slightly discharges to stabilize the system, causing the SOC to drop from about 70.0% to 69.9%. The bottom plot confirms that the PV inverter meets load demand steadily with minimal battery support, and the residual power stays near zero, indicating a stable, well-balanced operation. Battery charge–discharge behavior is presented in Fig. 15 and Fig. 16.

Fig. 16 shows the dynamic coordination among the PV system, battery, and load. In the upper plot, the battery alternates between discharging and charging modes, reflected by the slight variation in SOC near 70%, ensuring smooth energy flow. The lower plot highlights how the PV inverter delivers the main power to the load, while the battery adjusts its output to maintain system stability. The minimal residual power verifies that the combined PV and battery sources precisely balance the load demand.

Residual power remains close to zero in both Fig.15 and Fig.16, proving that PV and battery jointly maintain load balance with minimal mismatch. This confirms stable, well-coordinated energy management behavior.

The numerical differences observed between Model I (4 kW) and Model II (31.5 kW) arise from differences in system power rating, converter scaling, and dynamic load conditions. First, the higher power gain observed in Model II is primarily attributed to improved power transfer efficiency

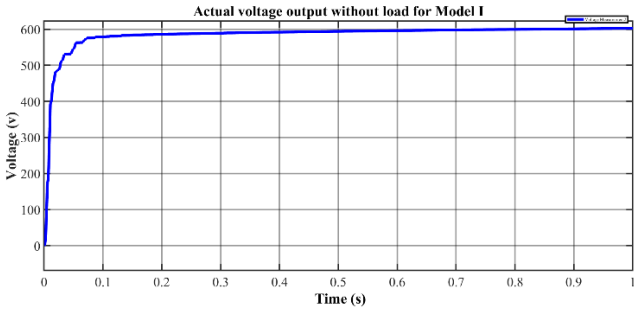

FIGURE 17. Actual voltage of proposed model I.

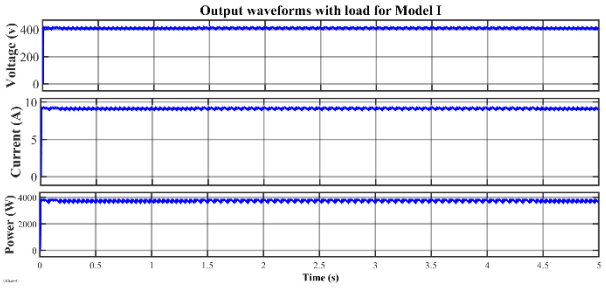

FIGURE 18. Output waveforms without buck converter for proposed model I.

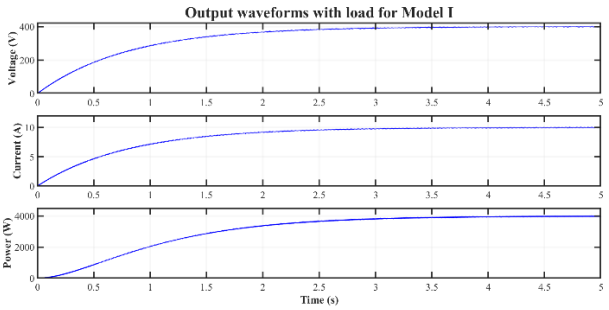

FIGURE 19. Output waveforms with buck converter for proposed model I.

at higher excitation levels. In resonant inductive systems, higher operating power levels reduce the relative impact of parasitic resistive losses (R1 and R2), thereby improving effective transfer efficiency. As a result, the 31.5 kW configuration achieves approximately 90.5% efficiency compared to 80% in the 4-kW configuration. Second, the variation in State of Charge (SoC) evolution between the two cases is directly related to charging power magnitude and battery capacity scaling. In Model I, the lower transmitted power results in a slower SoC increase under identical operating duration. In contrast, the higher-power configuration in Model II enables faster energy delivery to the EV battery, resulting in a steeper SoC rise. Additionally, under dynamic operation in Model II, coupling variation influences instantaneous power transfer. However, the higher available excitation power compensates for moderate coupling reduction, thereby sustaining overall charging performance. These results demonstrate that the proposed architecture remains scalable across power levels while preserving stable operation. The performance difference is therefore not a modeling inconsistency but a direct consequence of power rating, converter scaling, and resonant network behavior. From an infrastructure perspective, the 4 kW model is suitable for localized residential or modular deployment scenarios, whereas the 31.5 kW configuration supports corridor-level or fleet-based applications requiring higher throughput.

B. SIMULATION RESULT OF THREE-PHASE FAST CHARGING SYSTEM OF STATIC SINGLE-VEHICLE CHARGING WITH AND WITHOUT BUCK CONVERTER (PROPOSED MODEL I)

First, a simulation is performed with a capacitor alone to determine the actual transmission voltage; afterward, it is analyzed with a buck converter and a load. Simulation results and analysis of single-phase WCS with and without a buck converter are portrayed below.

Fig. 17 shows the actual WPT transmission voltage exceeding 600 V, demonstrating sufficient DC-link strength prior to power conditioning. When a load is directly applied without a buck converter (Fig. 18), the output settles around 400 V, 9.3 A, and ≈3.7 kW, although noticeable ripple and waveform disturbances are observed due to the absence of DC conditioning.

To address this, a buck converter is introduced (Fig. 19). The converter provides:

- smooth startup with no overshoot
- regulated output of ≈ 400 V
- steady current ≈ 9 A
- stable power ≈ 3.7–4.0 kW
- significantly reduced ripple

These results demonstrate improved power quality, reduced transient stress, and enhanced suitability for EV battery charging. The converter ensures controlled dynamics and better steady-state regulation, making the system reliably adaptable for static fast-charging applications.

C. SIMULATION RESULT OF THREE-PHASE CHARGING SYSTEM FOR STATIONARY AND DYNAMIC MULTIPLE-VEHICLE CHARGING MODES WITH AND WITHOUT BUCK CONVERTER(PROPOSED MODEL II)

Simulation observation criteria are the same as before, so the description isn't written separately. Simulation results of the proposed Model II are discussed below:

Since the three-phase system operates under balanced conditions, results are shown for a representative phase. Fig. 20 shows the actual WPT transmission voltage, while Fig. 21 presents load-connected behavior without the buck converter.

Although output levels near ≈890 V, 11.8 A, and ≈10.5 kW are achieved, the absence of regulation leads to noticeable ripple and transient oscillations, which are unsuitable for battery interfacing

With the buck converter enabled (Fig. 22), the output voltage rises smoothly to ≈880–900 V with negligible overshoot and minimal high-frequency ripple. Current stabilizes

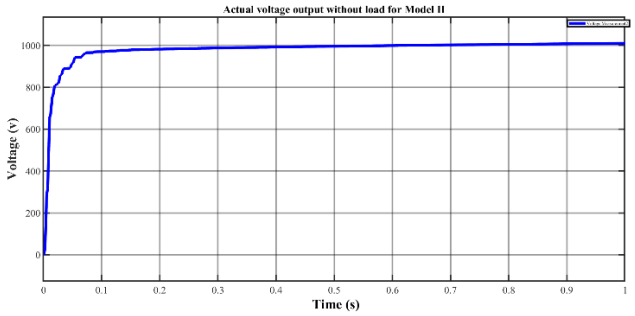

FIGURE 20. Actual output voltage of proposed model II.

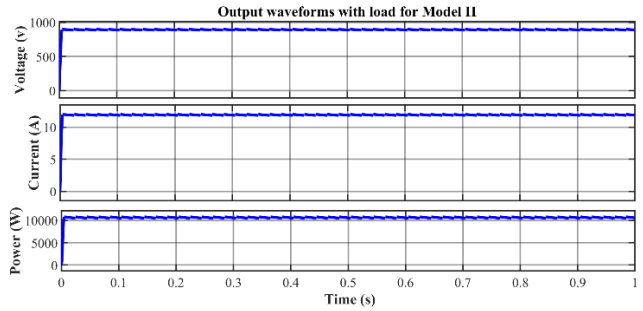

FIGURE 21. Output waveforms without the buck for proposed model II.

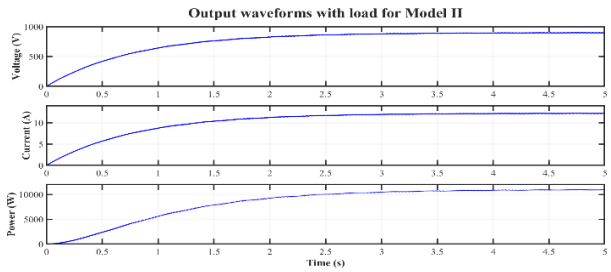

FIGURE 22. Output waveforms of the buck converter for proposed model II.

around 11–12 A, while output power remains consistently near ≈10.5 kW. These results confirm:

- effective damping
- controlled soft-start behavior
- reduced inrush stress
- improved DC stability
- enhanced EV charging suitability

Overall, the buck converter significantly improves waveform quality and regulation performance, ensuring reliable power delivery for both stationary and dynamic EV charging in Model II.

D. RESULT DISCUSSION

The simulation results comprehensively validate the technical feasibility, operational stability, and charging effectiveness of the proposed PV-integrated wireless charging system for electric vehicles. Across both Model I (static single-vehicle charging) and Model II (stationary and dynamic multi-vehicle charging), the PV arrays consistently delivered stable DC output, confirming effective MPPT regulation and the capability of the renewable source to sustain high-power charging demand. The inverter performance demonstrated balanced three-phase output with clean sinusoidal waveforms, establishing the suitability of the system for grid-compatible operation as well as inductive power transfer excitation. The battery response further confirms the robustness of the proposed hybrid architecture. The SOC fluctuated only minimally around 70%, demonstrating that the battery is not subjected to frequent deep cycling. This indicates improved battery lifespan, reliable power buffering, and stable power coordination between PV generation and the inverter. Residual power close to zero throughout operation verifies accurate load balancing and confirms that the proposed control strategy effectively stabilizes energy exchange during transitions.

A key observation is the significant improvement achieved with the integration of the DC–DC buck converter in both models. Without regulation, the output contained noticeable ripple and transient oscillations, which are unsuitable for direct EV battery interfacing [47]. After the buck converter application, the waveforms exhibit controlled soft-start behavior, negligible overshoot, reduced ripple, and steady-state stabilization at the required voltage and power levels. This enhancement demonstrates that the DC conditioning stage is essential to ensuring power quality, protecting downstream converters, and enabling safe, efficient, and battery-friendly charging. Such performance characteristics align with practical EV charging requirements and support conformity with wireless EV charging guidelines such as SAE J2954. Another important implication is scalability. Model I confirms suitability for household or single-vehicle public charging scenarios, while Model II demonstrates applicability for higher-power environments, including depots, fleet charging locations, and dynamic charging lanes. The smooth operational response in Model II proves that the proposed system remains reliable even under higher power stress and multi-vehicle operation, which is critical for future large-scale EV adoption in smart cities. From a broader perspective, the results highlight the system's ability to reduce stress on distribution grids by shifting charging demand toward locally generated renewable power. The architecture supports decentralized, modular deployment, making it suitable not only for developed urban smart-city infrastructures but also for developing regions, remote locations, and tourism-dependent areas where grid reliability may be limited. The demonstrated operational stability, renewable integration capability, and wireless charging convenience collectively indicate that the proposed system is a technically strong and practically scalable solution for sustainable urban mobility.

VII. OVERALL EFFICIENCY ANALYSIS

The efficiency evaluation summarizes the computed link-level (coil-to-coil) and end-to-end efficiencies of both proposed configurations using steady-state simulation data.

The analysis considers PV output, intermediate power-conditioning stages, WPT transmission, and regulated EV-side delivery.

For the three-phase static fast-charging configuration (Model I), the PV subsystem generated approximately 4.69 kW, while the regulated post-buck DC output stabilized around 3.75 kW, corresponding to an end-to-end efficiency of ≈ 80%. The Series–Series (SS) compensated inductive link demonstrated strong mutual coupling with limited reactive losses, achieving a coil-to-coil transfer efficiency of ≈ 91.7% at 85 kHz. Remaining losses are primarily attributed to conversion stages, including inverter switching, rectification, and DC buck regulation consistent with practical multi-stage wireless charging architectures.

For the higher-power stationary/dynamic charging configuration (Model II), each phase supplied approximately 10.5 kW of stable regulated DC, yielding a total EV-side delivery of ≈ 31.5 kW from an input PV power of ≈ 34.8 kW. This results in an overall efficiency of ≈ 90.5%, which is significantly higher than Model I. The performance improvement is attributed to better utilization of the converter ratings at higher loading conditions, reduced relative switching losses, and superior power-sharing consistency across the three phases. The balanced per-phase operating ranges (≈ 880–900 V and 11–12 A) further confirm stable and efficient system performance.

In both architectures, the buck converter played a key role in reducing ripple and stabilizing the DC output without introducing excessive efficiency penalties, while the SS compensation topology enabled resonant energy transfer with high coupling effectiveness. The obtained efficiencies are comparable to those of commercial SAE J2954 and IEC 61980-3 compliant wireless charging platforms [44], [45], verifying the technical feasibility of the proposed design. With further optimization, such as implementation of GaN-based high-frequency converters, reduced parasitic losses, and optimized filtering, the projected system efficiency can be increased beyond 92–94%, aligning with leading industry and laboratory benchmarks [48], [49].

VIII. WIRED AND WIRELESS CHARGING COMPARISON

Conventional wired charging remains the most widely deployed electric vehicle (EV) charging method due to its high efficiency and mature infrastructure. However, wired charging requires physical connectors, manual handling, and frequent plug–unplug operations, which introduce wear, safety concerns, and increased maintenance requirements, particularly in high-utilization environments such as public charging stations and fleet depots. In contrast, wireless power transfer (WPT) enables contactless energy delivery, eliminating exposed connectors and reducing mechanical degradation, environmental exposure, and user intervention, thereby improving operational reliability and user convenience [50].

From a system-level perspective, wired charging typically achieves slightly higher end-to-end efficiency because of fewer power-conversion stages. Nevertheless, recent advances in resonant compensation techniques, high-frequency power electronics, and control strategies have enabled wireless charging systems to achieve efficiencies exceeding 90%, approaching those of wired solutions while offering superior automation and robustness [51], [53]. In the proposed PV-integrated wireless charging system, the Series–Series (SS) compensated topology demonstrated coil-to-coil efficiencies of approximately 91.7% at an operating frequency of 85 kHz, which is consistent with efficiency levels reported for commercially oriented and standard-compliant wireless EV charging platforms.

TABLE 4. Comparison between wired and wirelesS EV charging systems.

Feature	Wired Charging	Wireless Charging (Proposed System)
Physical Contact	Required	Not required
User Intervention	Manual plug/unplug	Fully automatic
Maintenance	Higher (connector wear)	Lower
Safety	Risk of spark/exposure	Improved electrical isolation
Efficiency	Very high (≈95–98%)	High (≈90–92%)
Dynamic Charging	Not feasible	Feasible
Smart-City Integration	Limited flexibility	High suitability
Renewable Integration	Grid-centric	PV-integrated & decentralized

Wireless charging further enables automated and opportunity -based charging scenarios, including dynamic in-motion charging, autonomous vehicle charging, and fleet-based applications, which are impractical to realize using conventional wired charging infrastructure. When combined with renewable energy sources, wireless charging systems can be seamlessly integrated into smart-city environments, supporting sustainable mobility while reducing visual clutter and improving long-term system reliability [54]. Table 4 presents the comparison between the two charging systems.

This comparison highlights that although wired charging remains efficient, renewable-powered wireless charging provides superior flexibility, safety, and scalability for future smart-city and sustainable mobility applications.

IX. CHARGING TIME AND COST ANALYSIS

A. CHARGING TIME ESTIMATION

The charging time of an EV depends on the battery capacity, the state of charge (SoC) window, and the adequate charging power of the WCS. In this study, we consider a charging window of 20%–80% SoC, which reflects the practical range commonly adopted for battery longevity [44]. The required charging energy is given by:

$$\Delta E = c_{bat^x} \left(SoC_{final} - SoC_{initial} \right) \tag{21}$$

$$t = \frac{\Delta E}{P_{WPT} - \eta} \tag{22}$$

TABLE 5. The estimated charging times (20)–80% SOC).

EV Type	Energy Required (kWh)	Model I (3.75 kW)	Model II (10.5 kW)	SAE J2954 (3.7–11 kW)
PHEV (15 kWh)	9	2.40 h (2 h 24 min)	0.86 h (51 min)	0.8–2.4 h
Small BEV (40 kWh)	24	6.40 h	2.29 h (2 h 17 min)	2.2–6.5 h
BEV (60 kWh)	36	9.6 h	3.43 h (3 h 26 min)	3.3–10.8 h

TABLE 6. The estimated charging cost (20)–80% SOC).

EV Type	Energy Required (kWh)	Grid (€0.29/kWh)	PV Utility (€0.04/kWh)	PV Rooftop (€0.09/kWh)
PHEV (15 kWh)	9	€2.61	€0.36	€0.81
Small BEV (40 kWh)	24	€6.96	€0.96	€2.16
BEV (60 kWh)	36	€10.44	€1.44	€3.24

where P_{WPT} is the wireless transfer power, and η is the end-to-end efficiency.

- Battery sizes considered:
  - Plug-in hybrid EV (PHEV): 15 kWh → ΔE = 9 kWh
  - Small BEV: 40 kWh → $\Delta E = 24$ kWh
  - Standard BEV: 60 kWh → $\Delta E = 36$ kWh (IEA Global EV Outlook, 2023).
- Simulated model outputs:
  - Model I: ∼3.75 kW output
  - Model II: ∼10.5k W output

Commercial benchmark (SAE J2954): 3.7–11 kW wireless static charging levels. Table 5 summarizes the estimated charging durations (20)–80% SOC) for different EV types using Models I and II, along with SAE J2954 benchmarks.

B. COST ESTIMATION

Charging cost is determined by the energy required and the unit price of electricity from different sources:

$$Cost = \Delta E * C\ (unit) \tag{23}$$

- Grid electricity price (Finland, 2024): ∼€0.29/kWh (Eurostat).
- PV Levelized Cost of Energy (LCOE):
  a) Utility-scale PV: ∼ €0.04/kWh (IRENA, 2024)
  b) Rooftop PV: ∼ €0.08–0.09/kWh (European Commission JRC, 2024)

The corresponding charging cost estimates for various energy sources are presented in Table 6.

The comparative charging times and costs from Tables 5 and 6 are shown in Fig. 23.

Fig. 23, which summarizes the charging duration and cost variations across various vehicle types and energy sources, provides additional illustrations of the comparative results in Tables 5 and 6. The estimated charging time for the 20–80% SoC range using Model I (3.75 kW) and Model II (10.5 kW) is shown in the left sub-plot. As anticipated, the Model II's increased power capability allows for nearly three times faster charging, cutting the typical time for standard BEVs from roughly 9.6 hours to 3.4 hours. The related energy costs are shown in the right sub-plot under three pricing scenarios:

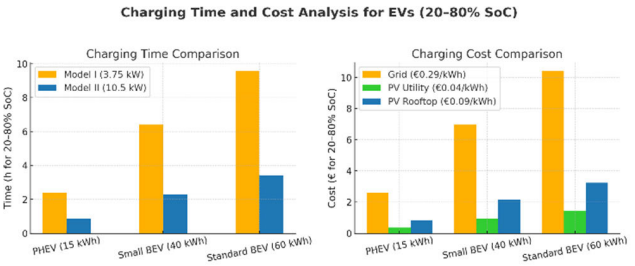

FIGURE 23. Charging Time and Cost Analysis for EVs (20)-80% SoC).

rooftop PV (€0.09/kWh), utility-scale PV (€0.04/kWh), and grid supply (€0.29/kWh). Compared with grid-only charging, integrating photovoltaic sources reduces charging costs by about 60% to 85%. These findings demonstrate that PV-integrated wireless charging can support demand-side flexibility in innovative urban energy systems by offering both operational and financial advantages.

The analysis confirms two critical insights:

1) TECHNICAL FEASIBILITY

Both models achieve high conversion efficiency across all power-conditioning stages, according to the simulation results. In line with state-of-the-art wireless charging benchmarks, the three-phase (3 single-phase) dynamic configuration (Model II) achieved 90% end-to-end efficiency, while the static fast-charging configuration (Model I) achieved about 80%. These efficiency trends attest to the feasibility of scaling the suggested PV-integrated architecture to higher power levels by leveraging advanced control algorithms, optimized resonant compensation, and wide-bandgap devices such as GaN- or SiC-based inverters. It is anticipated that these enhancements will increase overall system efficiency to 92%-94%, enabling dependable, high-power wireless EV charging in practical operating environments. [43]

2) SMART CITY RELEVANCE

The photovoltaic-based wireless charging system (WCS) reduces reliance on traditional grid electricity by providing a decentralized, sustainable charging pathway from a smart-city perspective. The system reduces peak-hour grid

demand, enhances local energy resilience, and facilitates integration with distributed energy resources (DERs) by drawing power directly from PV generation and battery storage. These charging stations can serve as bidirectional nodes in the urban energy network when widely installed, facilitating vehicle-to-grid (V2G) communication and demand response. Renewable-powered WCS hubs support clean mobility and grid flexibility, aligning with the larger smart-city goal of creating carbon-neutral, self-sustaining transportation infrastructure.

X. OVERALL PROPOSED SYSTEM

Within the context of smart cities, the suggested photovoltaic-integrated wireless charging systems (WCS) are made to accommodate both small- and large-scale e-mobility use cases.

Designed for single-vehicle fast charging in static mode, the three-phase static configuration (Model I) has a rating of about 4 kW. This configuration enables decentralized charging from renewable energy sources without relying on the grid, making it ideal for private or residential parking lots. This model guarantees dependable operation under fluctuating solar conditions by combining PV generation, maximum-power-point tracking (MPPT), and a bidirectional DC–DC interface with energy storage. The three-phase (3 × single-phase) stationary/dynamic configuration (Model II), on the other hand, has a higher power rating of about 31.5 kW (about 10.5 kW per phase). Parking lots, bus or taxi stops, and embedded road segments for dynamic charging are just a few of the public or commercial applications for which it is best suited.

This setup can serve as a distributed energy resource (DER) node in the smart grid and provide continuous energy transfer to multiple vehicles simultaneously. In doing so, it increases the share of renewable energy in urban mobility infrastructure, lowers peak-hour demand, and supports grid balancing. Fig. 24 illustrates all the operating modes of the proposed system and depicts their practical deployment scenarios in a clear and illustrative manner.

Together, these models highlight the adaptability of PV-integrated WCS across diverse urban contexts, from private households to large-scale smart-city transportation infrastructure. The main findings for both configurations, including PV ratings, efficiencies, and output power, are summarized in Table 6.

XI. COMPARATIVE PERFORMANCE ANALYSIS WITH RELATED WORKS

To highlight the achieved balance between efficiency, renewable autonomy, and multi-phase scalability, this section compares the proposed PV-integrated wireless charging configurations with representative state-of-the-art designs documented in the literature. Link efficiencies of roughly 91.7% are maintained by the suggested PV-integrated WCS configurations, which are on par with or better than those reported in earlier single-phase and grid-assisted studies [13], [17], [31],

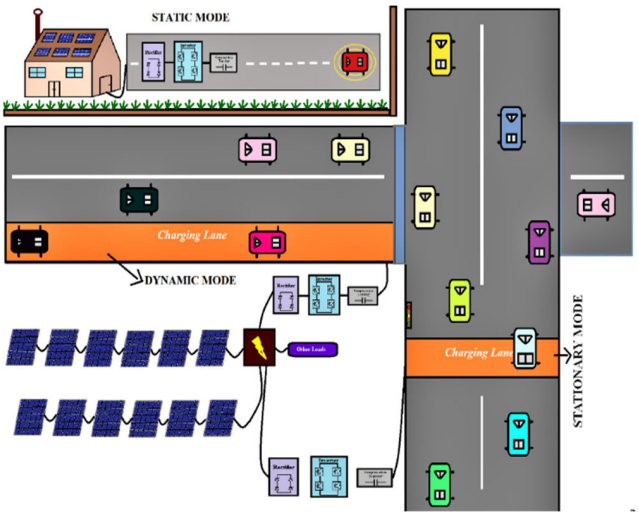

FIGURE 24. Overall proposed system.

TABLE 7. Overall proposed system.

Model	PV Rated Power (kW)	EV Output (Post-Buck)	Transfer Efficiency η_t (%)	End-to-End Efficiency η_e (%)
Model I	4.8	3.75 kW	91.7	80.0
Model II	34.8	10.5 kW per phase (≈ 31.5 kW total)	91.7	90.5

and [49]. Even though some lab prototypes under simplified grid-fed conditions achieve marginally higher absolute efficiencies, they usually do not include multi-phase operation, battery coupling, or renewable interfaces. In contrast, despite several power-conversion stages, the architecture presented combines photovoltaic generation, bidirectional storage, MPPT-based optimization, and three-phase dynamic transfer to achieve end-to-end efficiencies of up to 90.5%. This proves that the suggested models are appropriate for intelligent, scalable, and carbon-neutral mobility infrastructures in smart cities, as they operate as fully self-sustaining renewable systems and deliver performance comparable to that of an industrial system. The suggested multi-phase configurations show nearly equal transfer efficiency but significantly higher functional integration than earlier research. These models support both static and dynamic wireless operation, run solely on renewable energy, and provide bidirectional energy flow for vehicle-to-grid (V2G) compatibility. The uniqueness and scalability of the suggested architecture are highlighted by the fact that this system-level combination of PV generation, energy storage, and wireless transfer at the multi-kilowatt scale has never been documented

TABLE 8. Comparative performance of the proposed PV-Integrated WCS with recent works.

Study	System Configuration	Rated Power (kW)	Link η (%)	End-to-End η (%)	Distinctive Features / Limitations
Gaddam et al. (2022) [26]	PV-fed grid-assisted single-phase WPT	3.3	90	87	Grid-tied; no battery storage or dynamic mode
Li et al. (2017) [14]	Dual Tx/Rx resonant WPT	6.6	93	88	High link η; lacks renewable integration
Farghly et al. (2025) [46]	GaN-based inverter WPT prototype	6.6	94	—	Hardware test; no renewable coupling
Ahmad et al. (2018) [12]	Conventional single-phase WPT	3.7	89	83	Static; fixed coupling; grid-fed
Proposed Model I	PV–Battery–MPPT–SS WPT (Static)	**4.8**	**91.7**	**80.0**	**Renewable, self-sustained, bidirectional control**
Proposed Model II	PV–Battery–MPPT–3Φ WPT (Stationary and Dynamic)	**34.8**	**91.7**	**90.5**	**Renewable-integrated, dynamic, scalable, smart-grid-ready,**

before. Comparative performance of the proposed PV-integrated WCS with recent works is shown in Table 8.

The comparative findings summarized above validate that the proposed PV-integrated WCS delivers industrial-grade efficiency while achieving renewable independence and scalability unmatched in prior studies.

XII. FUTURE WORK

Future research will focus on extending the proposed photovoltaic-integrated wireless charging system toward practical deployment and enhanced operational intelligence. Although the present work demonstrates the feasibility of the proposed architecture through detailed MATLAB/Simulink simulations, experimental validation remains an important next step. Therefore, future work will involve the development of a hardware prototype to experimentally validate the PV–battery–wireless power transfer (WPT) architecture under real operating conditions.

Further investigation will also focus on improving system efficiency and power density by employing wide-bandgap semiconductor devices such as gallium nitride (GaN) or silicon carbide (SiC) converters. These technologies can significantly reduce switching losses and enable higher-frequency operation, which is particularly beneficial for wireless power transfer systems operating near the standardized 85 kHz frequency band.

Another promising direction involves the integration of advanced control strategies and intelligent energy management. Artificial intelligence (AI) and machine learning techniques could be applied to predict solar generation, optimize battery dispatch, and dynamically regulate charging power under varying environmental and load conditions. Such predictive control strategies could improve system reliability and maximize renewable energy utilization.

In addition, future studies will explore Internet-of-Things (IoT) based monitoring and communication frameworks to enable real-time system supervision, remote diagnostics, and integration with smart-grid infrastructures. This capability would allow wireless charging stations to operate as distributed energy resources (DERs) within smart-city energy networks, supporting demand response and vehicle-to-grid (V2G) interaction.

Finally, further work will investigate the scalability of the proposed system for higher-power EV charging infrastructures and alignment with international wireless charging standards such as SAE J2954 and IEC 61980. These studies will support the practical implementation of renewable-powered wireless charging networks for sustainable and resilient urban mobility

XIII. CONCLUSION

This study presented a comprehensive photovoltaic (PV)-integrated wireless charging system (WCS) for electric vehicles, validated through detailed MATLAB/Simulink simulations. Two scalable configurations were designed and analyzed to promote sustainable mobility within smart-city environments: a three-phase static fast-charging system (Model I) rated at approximately 4 kW for residential single-vehicle applications, and a three-phase stationary/dynamic charging system (Model II), delivering approximately 31.5 kW in total (≈10.5 kW per phase), suitable for public transport and multi-vehicle charging scenarios. Both configurations integrate PV generation with maximum power point tracking (MPPT), bidirectional DC–DC conversion with battery energy storage, and a series–series (SS) compensated wireless power transfer network operating near 85 kHz.

Simulation results confirmed stable operation across all power-conditioning stages and operating modes. The SS compensation topology achieved a coil-to-coil transfer efficiency of approximately 91.7%, while the overall end-to-end efficiencies of Model I and Model II were approximately 80% and 90%, respectively. The inclusion of a DC–DC buck converter significantly improved output power quality by ensuring smooth voltage and current regulation, enabling stable and battery-friendly charging behavior. In addition, the integrated Battery Management System (BMS) effectively coordinated charging and discharging actions, maintained a stable state of charge, and enhanced system reliability and battery lifetime.

Beyond technical performance, the proposed PV-integrated WCS demonstrates strong practical relevance. The results indicate that renewable-powered wireless charging can flexibly support a wide range of applications, from low-power residential charging to high-power dynamic public transportation scenarios. Techno-economic evaluation further suggests that PV-based wireless charging infrastructures can reduce energy costs by approximately 60–85% compared to grid-dependent charging, while simultaneously alleviating

stress on urban distribution networks. From a smart-grid perspective, the proposed system can operate as a distributed energy resource (DER), supporting demand-response strategies and enabling future vehicle-to-grid (V2G) participation.

Despite these promising results, certain limitations remain. The present work is based on simulation-scale models, and experimental validation has not yet been performed. In addition, while the system architecture is scalable, further investigation is required to assess performance at higher power levels and under real-world operating uncertainties. Future work will therefore focus on hardware prototyping, real-time controller implementation, and experimental testing. Planned extensions include the use of GaN-based power converters to improve efficiency and power density, IoT-enabled monitoring for enhanced system supervision, and AI-driven adaptive control strategies for predictive energy management. Alignment with SAE J2954 power classes (3.7–11 kW and above) will further strengthen the system's readiness for commercial EV charging infrastructure.

In conclusion, the proposed PV-integrated wireless charging system offers a technically robust, economically viable, and environmentally sustainable pathway toward carbon-neutral transportation. By combining photovoltaic generation, wireless power transfer, energy storage, and intelligent control, the presented framework directly supports the development of resilient, decentralized, and renewable-powered mobility ecosystems for next-generation smart cities.

ACKNOWLEDGMENT

The authors used AI-based language tools, including Grammarly, QuillBot, and ChatGPT, solely for improving grammar, spelling, and phrasing during manuscript preparation. The scientific ideas, simulations, analyses, and conclusions presented in this article are entirely the authors' original contributions. All responsibility for the content rests with the authors.

REFERENCES

[1] Environmental Protection Agency (EPA). (2019). *Global Greenhouse Gas Emissions Data*. [Online]. Available: https://www.epa.gov/ghgemissions/global-greenhouse-gas-emissions-data

[2] H. Ritchie and M. Roser, "CO_2 and other greenhouse gas emissions," *Our World in Data*, 2019. [Online]. Available: https://ourworldindata.org/co2-and-other-greenhouse-gas-emissions

[3] A. P. Aizebeokhai, "Global warming and climate change: Realities uncertainties and measures," *Int. J. Phys. Sci.*, vol. 4, no. 13, pp. 868–879, 2009.

[4] IPCC, "Climate change 2014: Mitigation of climate change," Contribution of Working Group III to the Fifth Assessment Report of the Intergovernmental Panel on Climate Change, Cambridge Univ. Press, Cambridge, U.K., Tech. Rep., 2014.

[5] A. Rakhymbay, M. Bagheri, and M. Lu, "A simulation study on four different compensation topologies in EV wireless charging," in *Proc. Int. Conf. Sustain. Energy Eng. Appl. (ICSEEA)*, Oct. 2017, pp. 66–73, doi: 10.1109/icseea.2017.8267689.

[6] A. Triviño, J. M. González-González, and J. A. Aguado, "Wireless power transfer technologies applied to electric vehicles: A review," *Energies*, vol. 14, no. 6, p. 1547, Mar. 2021, doi: 10.3390/en14061547.

[7] Z. Xue, W. Liu, C. Liu, and K. T. Chau, "Critical review of wireless charging technologies for electric vehicles," *World Electric Vehicle J.*, vol. 16, no. 2, p. 65, Jan. 2025, doi: 10.3390/wevj16020065.

[8] *Wireless EV Taxi Trial in Gothenburg*, Project Report, Volvo Cars, Sweden, 2021.

[9] *Bus Charging Infrastructure Case Study*, ElectriCity Gothenburg, Gothenburg, Sweden, 2022.

[10] G. A. Covic and J. T. Boys, "Inductive power transfer," *Proc. IEEE*, vol. 101, no. 6, pp. 1276–1289, Jun. 2013.

[11] J. Hu, H. Morais, T. Sousa, and M. Lind, "Electric vehicle fleet management in smart grids: A review of services, optimization and control aspects," *Renew. Sustain. Energy Rev.*, vol. 56, pp. 1207–1226, Apr. 2016, doi: 10.1016/j.rser.2015.12.014.

[12] A. Ahmad, M. S. Alam, and R. Chabaan, "A comprehensive review of wireless charging technologies for EVs," *IEEE Trans. Transport. Electrific.*, vol. 4, no. 1, pp. 38–63, Nov. 2018.

[13] SAE International, "SAE j2954: Wireless power transfer for light-duty plug-in/electric vehicles and alignment methodology," SAE International, Warrendale, PA, USA, Tech. Rep. SAE J2954, 2022.

[14] Y. Li, R. Mai, T. Lin, H. Sun, and Z. He, "A novel WPT system based on dual transmitters and dual receivers for high power applications," *Energies*, vol. 10, p. 174, Feb. 2017.

[15] A. Ghosh, A. Ukil, and A. P. Hu, "Integration of rooftop solar PV generation with wireless power transfer," in *Proc. IEEE PES APPEEC*, Dec. 2019, pp. 1–5, doi: 10.1109/APPEEC45492.2019.8994668.

[16] *Renewables 2025: Analysis and Forecast To 2030*, International Energy Agency (IEA), Paris, 2025.

[17] *Global EV Outlook 2023*, International Energy Agency (IEA), Paris, 2023.

[18] *Electricity Prices for Household Consumers–Semi-annual Data*, Eur. Commission, Luxembourg, 2024.

[19] *Renewable Power Generation Costs in 2024*, IRENA, Abu Dhabi, 2025.

[20] *Newables 2024: Analysis and Forecast To 2030*, International Energy Agency (IEA), Paris, France, 2024.

[21] M. Rabih, M. Takruri, M. Al-Hattab, A. A. Alnuaimi, and M. R. Bin Thaleth, "Wireless charging for electric vehicles: A survey and comprehensive guide," *World Electric Vehicle J.*, vol. 15, no. 3, p. 118, Mar. 2024, doi: 10.3390/wevj15030118.

[22] A. Atia, F. Anayi, and M. Gao, "Influence of shading on solar cell parameters and modelling accuracy," *Energies*, vol. 15, no. 23, p. 9067, 2022.

[23] W. Chen, J. Ren, T. Chen, Z. Xu, N. Nick, S. Chen, X. Wu, J. Lin, C. Zhao, and Y. Liu, "The impact of haze on photovoltaic systems: A case study," *Energy Sour., Part A: Recovery, Utilization, Environ. Effects*, vol. 47, no. 1, pp. 7017–7032, Jun. 2025.

[24] T. S. Chandrasekar Rao and K. Geetha, "Categories, standards and recent trends in wireless power transfer: A survey," *Indian J. Sci. Technol.*, vol. 9, no. 20, pp. 1–11, May 2016.

[25] K. Deepti, P. Srihari, and M. Achari, "MPPT based auto integrated dust control and efficient cooling mechanism for PV," *Indian J. Sci. Technol.*, vol. 9, no. 31, pp. 1–7, 2016.

[26] S. Gaddam, S. Yasam, and N. Ranjit, "Wireless electric vehicle battery charging system using PV array," *Int. J. Res. Appl. Sci. Eng. Technol.*, vol. 10, no. 6, Jun. 2022, doi: 10.22214/ijraset.2022.43916.

[27] F. Liu, Y. Kang, Y. Zhang, and S. Duan, "Comparison of P&O and Hill climbing MPPT methods for grid-connected PV converter," in *Proc. 3rd IEEE Conf. Ind. Electron. Appl.*, Jun. 2008, pp. 804–807.

[28] Z. Arif, V. Ravikiran, and R. Kumar Keshri, "Design of PV fed wireless charger for electric vehicle," in *Proc. Int. Conf. Power Electron. IoT Appl. Renew. Energy its Control (PARC)*, Feb. 2020, pp. 303–307.

[29] A. Kurs, A. Karalis, R. Moffatt, J. D. Joannopoulos, P. Fisher, and M. Soljačić, "Wireless power transfer via strongly coupled magnetic resonances," *Science*, vol. 317, no. 5834, pp. 83–86, Jul. 2007.

[30] H. Hao, G. Covic, and J. T. Boys, "An approximate dynamic model of LCL-T-based inductive power transfer power supplies," *IEEE Trans. Power Electron.*, vol. 29, no. 10, pp. 5554–5567, Oct. 2014.

[31] S. Mandal et al., "Motion prediction for autonomous vehicles using deep learning," in *Proc. IEEE Int. Conf. Comput. Commun. Autom. (ICCCA)*, Jul. 2023, pp. 768–773.

[32] A. Soni, D. Dharmacharya, A. Pal, V. K. Srivastava, R. N. Shaw, and A. Ghosh, "Design of a machine learning-based self-driving car," in *Machine Learning for Robotics Applications*. Singapore: Springer, 2021, pp. 139–151.

[33] S. Li and C. C. Mi, "Wireless power transfer for electric vehicle applications," *IEEE J. Emerg. Sel. Topics Power Electron.*, vol. 3, no. 1, pp. 4–17, Mar. 2015, doi: 10.1109/JESTPE.2014.2319453.

[34] T. Ching and Y. Wong, "Review of wireless charging technologies for EVs," in *Proc. Int. Conf. Power Electron. Syst. Appl. (PESA)*, Hong Kong, 2013, pp. 1–4.
[35] P. Palimkar, V. Bajaj, A. Mal, R. N. Shaw, and A. Ghosh, "Unique action identifier using sensors," in *Advanced Computing and Intelligent Technologies* (Lecture Notes in Networks and Systems), vol. 218, M. Bianchini, V. Piuri, S. Das, and R. N. Shaw, Eds., Singapore: Springer, 2022, doi: 10.1007/978-981-16-2164-2_48.
[36] J. Li, F. Yin, and L. Wang, "Transmission efficiency of shielding structures in WPT systems for EVs," *CSEE J. Power Energy Syst.*, vol. 7, no. 6, pp. 1247–1255., 2021.
[37] K. Zhou, Y. Wu, X. Wu, Y. Sun, D. Teng, and Y. Liu, "Research and development review of power converter topologies and control technology for electric vehicle fast-charging systems," *Electronics*, vol. 12, no. 7, p. 1581, Mar. 2023, doi: 10.3390/electronics12071581.
[38] M. Howaidi and Y. Mahmoud, "A comprehensive review of wireless charging systems for automated guided vehicles," *IEEE Access*, vol. 14, pp. 5821–5854, 2026, doi: 10.1109/ACCESS.2026.3650869.
[39] G. Zhu and D. Gao, "Optimal load impedance in LCC-compensated IPT systems," *eTransportation*, vol. 11, Feb. 2022, Art. no. 100153.
[40] T. A. Shikdar, S. Dey, S. Mumtahina, M. M. Rashid, and G. M. Chowdhury, "Design and simulation of single phase and three phase wireless power transfer in electric vehicle using MATLAB/Simulink," in *Innovations in Electrical and Electronic Engineering* (Lecture Notes in Electrical Engineering), vol. 894, S. Mekhilef, R. N. Shaw, and P. Siano, Eds., Singapore: Springer, 2022, doi: 10.1007/978-981-19-1677-9_8.
[41] S. H. Ahmed and I. Ahmad, "Optimal wireless power transfer to hybrid energy storage system for electric vehicles: A comparative analysis of machine learning-based model-free controllers," *J. Energy Storage*, vol. 75, Jan. 2024, Art. no. 109534, doi: 10.1016/j.est.2023.109534.
[42] *Photovoltaic LCOE in Europe 2024: Rooftop and Utility-scale Assessment*, European Commission JRC, Brussels, 2024.
[43] M. H. Alsharif, F. Alsaif, M. K. Singla, S. Manna, and M.-K. Kim, "Techno-economic optimization and environmental analysis of a solar-powered electric vehicles (EVs) charger system for a greener transportation ecosystem," *Energy Rep.*, vol. 13, pp. 5803–5814, Jun. 2025, doi: 10.1016/j.egyr.2025.05.040.
[44] H. S. E. Mansour, M. Samir, B. Elhady, and S. Abdelmaksoud, "Wireless charging systems for electric vehicles: Review," *Green Energy Intell. Transp.*, vol. 1, Nov. 2025, Art. no. 100371, doi: 10.1016/j.geits.2025.100371.
[45] S. S. Sobhani, R. Zahedi, H. Yousefi, and A. Hajinezhad, "Configuring renewable energy supply for electric vehicle charging stations in Switzerland: Life cycle assessment and multi-objective optimization," *Energy Convers. Manage., X*, vol. 29, 2026, Art. no. 101457, 2026, doi: 10.1016/j.ecmx.2025.101457.
[46] A. Farghly, A. Mohamed, H. Awad, S. Abdelfatah, M. A. Alharbi, M. Alqarni, and S. Ali Abdelrazik, "A comprehensive review of wireless power transfer techniques for electric vehicle charging," *IEEE Access*, vol. 13, pp. 199683–199718, 2025, doi: 10.1109/ACCESS.2025.3635408.
[47] B. Hauke, "Basic calculation of a boost converter's power stage," Texas Instrum., Application Report SLVA372D, Nov. 2022.
[48] G. Ramkumar, S. Kannan, V. Mohanavel, S. Karthikeyan, and A. Titus, "The future of green mobility: A review exploring renewable energy systems integration in electric vehicles," *Results Eng.*, vol. 27, Sep. 2025, Art. no. 105647, doi: 10.1016/j.rineng.2025.105647.
[49] H. Bludszuweit, "Project Victoria–The first Spanish showcase for DWPT," in *Proc. FABRIC Conf.*, Brussels, 2016.
[50] T. A. Shikdar, M. M. Rashid, F. B. Ayub, and S. Faisal, "Development of automated protection and monitoring system for poor railway infrastructure," in *Proc. Int. Conf. Commun., Comput. Electron. Syst.*, vol. 844, Springer, 2022.
[51] S. Abilash, A. J. Abinesh, and M. Balaji, "Dynamic wireless charging for E-vehicles," in *Proc. 1st Int. Conf. Res. Develop. Inf., Commun. Comput. Technol. (ICRDICCT)*, 2025, pp. 760–766, doi: 10.5220/0013889600004919.
[52] N. Mohamed, F. Aymen, T. E. A. Alharbi, C. Z. El-Bayeh, S. Lassaad, S. S. M. Ghoneim, and U. Eicker, "A comprehensive analysis of wireless charging systems for electric vehicles," *IEEE Access*, vol. 10, pp. 43865–43881, 2022, doi: 10.1109/ACCESS.2022.3168727.
[53] O. Abuajwa, S. P. Thiagarajah, Z. Ambak, M. T. Sarker, G. Ramasamy, and A. P. David, "Comprehensive review of wireless power transfer systems for electric vehicle charging applications," in *Discover Applied Sciences*, vol. 7. Cham, Switzerland: Springer, 2025, Art. no. 1176, doi: 10.1007/s42452-025-07738-z.
[54] P. Chowdhury, M. M. Alom Shovon, R. Yeassin, and O. Farrok, "Wireless charging for electric vehicles: A review on environmental, health, technical, and policy landscape," *Energy Convers. Management: X*, vol. 28, Oct. 2025, Art. no. 101363, doi: 10.1016/j.ecmx.2025.101363.

TAREQ ANWAR SHIKDAR received the B.Sc. degree (Hons.) in electrical and electronic engineering from Leading University, Bangladesh. He was a Erasmus Scholar. He is currently pursuing the Erasmus Mundus Joint Master Degree in Smart Cities and Communities (SMACCs), specializing in smart grid solutions with the University of Vaasa, Finland, with prior specializations in energy efficiency in buildings with the University of the Basque Country (UPV/EHU), Spain, and in information and communication technologies with the International Hellenic University (IHU), Greece. He has authored several publications in Springer Lecture Notes and international conferences, including ICEEE, ICCCES, and IC4IR, and serves as a reviewer for IEEE-indexed conferences. His professional experience includes lecturing and research in energy systems and robotics laboratories. His research interests include smart grids, renewable integration, battery energy storage, AI-based energy management, and the IoT-enabled predictive analytics.

HANNU LAAKSONEN (Member, IEEE) received the M.Sc. (Tech.) degree in electrical power engineering from Tampere University of Technology, Tampere, Finland, in 2004, and the Ph.D. (Tech.) degree in electrical engineering from the University of Vaasa, Vaasa, Finland, in 2011. His employment experience includes working as a Research Scientist with the VTT Technical Research Centre of Finland and the University of Vaasa. He has previously worked as a Principal Engineer with ABB Ltd., Vaasa. He is currently a Professor of electrical engineering with the University of Vaasa. He is also with the Electrical Engineering Department, PU-Manager, Flexible Energy Resources-Research Team Leader and the Manager of the Smart Energy Transition Master's Program. His research interests include the control and protection of low-inertia power systems and microgrids, active management of distributed and flexible energy resources in future smart energy systems, and future-proof technology and market concepts for smart grids.